

1 **Limitations of principal components in quantitative genetic**
2 **association models for human studies**

3 Yiqi Yao,^{1,3} Alejandro Ochoa^{1,2,*}

4 ¹ Department of Biostatistics and Bioinformatics, Duke University, Durham, NC 27705, USA

5 ² Duke Center for Statistical Genetics and Genomics, Duke University, Durham, NC 27705, USA

6 ³ Present address: BenHealth Consulting, Shanghai, Shanghai, 200023, China

7 * Correspondence: alejandro.ochoa@duke.edu

8 **Abstract**

9 Principal Component Analysis (PCA) and the Linear Mixed-effects Model (LMM), some-
10 times in combination, are the most common genetic association models. Previous PCA-LMM
11 comparisons give mixed results, unclear guidance, and have several limitations, including not
12 varying the number of principal components (PCs), simulating simple population structures,
13 and inconsistent use of real data and power evaluations. We evaluate PCA and LMM both
14 varying number of PCs in realistic genotype and complex trait simulations including admixed
15 families, trees, and real multiethnic human datasets with simulated traits. We find that LMM
16 without PCs usually performs best, with the largest effects in family simulations and real human
17 datasets and traits without environment effects. Poor PCA performance on human datasets is
18 driven by large numbers of distant relatives more than the smaller number of closer relatives.
19 While PCA was known to fail on family data, we report strong effects of family relatedness in
20 genetically diverse human datasets, not avoided by pruning close relatives. Environment effects
21 driven by geography and ethnicity are better modeled with LMM including those labels instead
22 of PCs. This work better characterizes the severe limitations of PCA compared to LMM in
23 modeling the complex relatedness structures of multiethnic human data for association studies.

24 **Abbreviations:** PCA: principal component analysis; PCs: principal components; LMM: linear
25 mixed-effects model; FES: fixed effect sizes (trait model); RC: random coefficients (trait model);

26 MAF: minor allele frequency; WGS: whole genome sequencing.

27 1 Introduction

28 The goal of a genetic association study is to identify loci whose genotype variation is significantly
29 correlated to given trait. Naive association tests assume that genotypes are drawn independently
30 from a common allele frequency. This assumption does not hold for structured populations, which
31 includes multiethnic cohorts and admixed individuals (ancient relatedness), and for family data
32 (recent relatedness) [1]. When insufficient approaches are applied to data with relatedness, their
33 association statistics are miscalibrated, resulting in excess false positives and loss of power [1–
34 3]. Therefore, many specialized approaches have been developed for genetic association under
35 relatedness, of which PCA and LMM are the most popular.

36 Genetic association with PCA consists of including the top eigenvectors of the population kin-
37 ship matrix as covariates in a generalized linear model [4–6]. These top eigenvectors are commonly
38 referred to as PCs in genetics [7], the convention adopted here, but in other fields PCs denote the
39 projections of loci onto eigenvectors [8]. The direct ancestor of PCA association is structured as-
40 sociation, in which inferred ancestry or admixture proportions are used as regression covariates [9].
41 These models are deeply connected because PCs map to ancestry empirically [10, 11] and theoreti-
42 cally [12–15], and they work as well as global ancestry in association studies but are estimated more
43 easily [6, 7, 10, 16]. PCs are also proposed for modeling environment effects that are correlated
44 to ancestry, for example, through geography [17–19]. The strength of PCA is its simplicity, which
45 as covariates can be readily included in more complex models, such as haplotype association [20]
46 and polygenic models [21]. However, PCA assumes that relatedness is low-dimensional, which may
47 limit its applicability. PCA is known to be inadequate for family data [7, 22, 23], which is called
48 “cryptic relatedness” when it is unknown to the researchers, but no other troublesome cases have
49 been confidently identified. Recent work has focused on developing more scalable versions of the
50 PCA algorithm [24–28]. PCA remains a popular and powerful approach for association studies.

51 The other dominant association model under relatedness is the LMM, which includes a random
52 effect parametrized by the kinship matrix. Unlike PCA, LMM does not assume that relatedness

53 is low-dimensional, and explicitly models families via the kinship matrix. Early LMMs required
54 kinship matrices estimated from known pedigrees or which otherwise captured recent relatedness
55 only [16, 29]. Modern LMMs estimate kinship from genotypes using a non-parametric estimator,
56 often referred to as a genetic relationship matrix, that captures the combined covariance due to
57 recent family relatedness and ancestral population structure [1, 30, 31]. Like PCA, LMM has also
58 been proposed for modeling environment correlated to genetics [32, 33]. The classic LMM assumes
59 a quantitative (continuous) complex trait, the focus of our work. Although case-control (binary)
60 traits and their underlying ascertainment are theoretically a challenge [34], LMMs have been applied
61 successfully to balanced case-control studies [1, 35] and simulations [23, 36, 37], and have been
62 adapted for unbalanced case-control studies [38]. However, LMMs tend to be considerably slower
63 than PCA and other models, so much effort has focused on improving their runtime and scalability
64 [30, 35, 38–46].

65 An LMM variant that incorporates PCs as fixed covariates is tested thoroughly in our work.
66 Since PCs are the top eigenvectors of the same kinship matrix estimate used in modern LMMs [1,
67 18, 47], then population structure is modeled twice in an LMM with PCs. However, some previous
68 work has found the apparent redundancy of an LMM with PCs beneficial [18, 23, 48], while others
69 did not [49], and the approach continues to be used [50, 51]. (Recall that early LMMs used kinship
70 to model family relatedness only, so population structure had to be modeled separately, in practice
71 as admixture fractions instead of PCs [16, 29].) The LMM with PCs (vs no PCs) is believed to help
72 better model loci that have experienced selection [23, 32] and environment effects correlated with
73 genetics [18].

74 LMM and PCA are closely related models [1, 18, 47], so similar performance is expected par-
75 ticularly under low-dimensional relatedness. Direct comparisons have yielded mixed results, with
76 several studies finding superior performance for LMM (notably from papers promoting advances in
77 LMMs) while many others report comparable performance (Table 1). No papers find that PCA
78 outperforms LMM decisively, although PCA occasionally performs better in isolated and artificial
79 cases or individual measures (often with unknown significance). Previous studies were generally
80 divided those that employed simulated versus real genotypes (only one study used both). The

81 simulated genotype studies, which tended to have low dimensionalities and differentiation (F_{ST}),
 82 were more likely to report ties or mixed results (6/7), whereas real genotypes tended to clearly
 83 favor LMMs (7/9). Similarly, 8/10 papers with quantitative traits favor LMMs, whereas 6/8 papers
 84 with case-control traits gave ties or mixed results (the only factor we do not explore). Additionally,
 85 although all previous evaluations measured type I error (or proxies such as inflation factors or QQ
 86 plots), a large fraction (6/15) did not measure power (including proxies such as ROC curves), and
 87 only three used more than one number of PCs for PCA. Lastly, no consensus has emerged as to why
 88 LMM might outperform PCA or vice versa [23, 37, 47, 55], or which features of the real datasets
 89 are critical for the LMM advantage other than cryptic relatedness, resulting in unclear guidance
 90 for using PCA. Hence, our work includes real and simulated genotypes with higher dimensionalities
 91 and differentiation matching that of multiethnic human cohorts, we vary the number of PCs, and
 92 measure robust proxies for type I error control and calibrated power.

Table 1: Previous PCA-LMM evaluations in the literature.

Publication	Sim. Genotypes			Real ^d	Trait ^e	Power	PCs (r)	Best
	Type ^a	K^b	F_{ST}^c					
Zhao et al. [16]				✓	Q	✓	8	LMM
Astle and Balding [1]	I	3	0.10		CC	✓	10	Tie
Kang et al. [35]				✓	Both		2-100	LMM
Price et al. [23]	I, F	2	0.01		CC		1	Mixed
Wu et al. [36]	I, A	2-4	0.01		CC	✓	10	Mixed
Liu et al. [49]	S, A	2-3	R		Q	✓	10	Tie
Sul and Eskin [37]	I	2	0.01		CC		1	Tie
Tucker, Price, and Berger [48]	I	2	0.05	✓	Both	✓	5	Tie
Yang et al. [34]				✓	CC	✓	5	Tie
Song, Hao, and Storey [52]	S, A	2-3	R		Q		3	LMM
Loh et al. [46]				✓	Q	✓	10	LMM
Zhang and Pan [18]				✓	Q	✓	20-100	LMM
Liu et al. [53]				✓	Q	✓	3-6	LMM
Sul, Martin, and Eskin [54]				✓	Q		100	LMM
Mbatchou et al. [51]				✓	Both		1	LMM
This work	A, T, F	10-243	≤ 0.25	✓	Q	✓	0-90	LMM

^aGenotype simulation types. I: Independent subpopulations; S: subpopulations (with parameters drawn from real data); A: Admixture; T: Tree; F: Family.

^bModel dimensionality (number of subpopulations or ancestries)

^cR: simulated parameters based on real data, F_{ST} not reported.

^dEvaluations using unmodified real genotypes.

^eQ: quantitative; CC: case-control.

93 In this work, we evaluate the PCA and LMM association models under various numbers of
 94 PCs (included in LMM too). We use genotype simulations (admixture, family, and tree models)
 95 and three real datasets: the 1000 Genomes Project [56, 57], the Human Genome Diversity Panel
 96 (HGDP) [58–60], and Human Origins [61–64]. We simulate quantitative traits from two models:
 97 fixed effect sizes (FES; coefficients inverse to allele frequency) that matches real data [50, 65, 66] and
 98 corresponds to high pleiotropy and strong balancing selection [67] and strong negative selection [50,
 99 66], which are appropriate assumptions for diseases; and random coefficients (RC; independent of
 100 allele frequency) that corresponds to neutral traits [50, 67]. LMM without PCs consistently performs
 101 best in simulations without environment, and greatly outperforms PCA in the family simulation
 102 and in all real datasets. The tree simulations do not recapitulate the real data results, suggesting
 103 that family relatedness in real data is the reason for poor PCA performance. Lastly, removing up
 104 to 4th degree relatives in the real datasets recapitulates poor PCA performance, showing that the
 105 more numerous distant relatives explain the result, and suggesting that PCA is generally not an
 106 appropriate model for real data. We find that both LMM and PCA are able to model environment
 107 effects correlated with genetics, and LMM with PCs gains a small advantage in this setting only, but
 108 direct modeling of environment performs much better. All together, we find that LMMs without PCs
 109 are generally a preferable association model, and present novel simulation and evaluation approaches
 110 to measure the performance of these and other genetic association approaches.

111 2 Materials and Methods

112 2.1 The complex trait model and PCA and LMM approximations

113 Let $x_{ij} \in \{0, 1, 2\}$ be the genotype at the biallelic locus i for individual j , which counts the number
 114 of reference alleles. Suppose there are n individuals and m loci, $\mathbf{X} = (x_{ij})$ is their $m \times n$ genotype
 115 matrix, and \mathbf{y} is the length- n (column) vector of individual trait values. The additive linear model
 116 for a quantitative (continuous) trait is:

$$117 \quad \mathbf{y} = \mathbf{1}\alpha + \mathbf{X}^\top \boldsymbol{\beta} + \mathbf{Z}^\top \boldsymbol{\eta} + \boldsymbol{\epsilon}, \quad (1)$$

118 where $\mathbf{1}$ is a length- n vector of ones, α is the scalar intercept coefficient, $\boldsymbol{\beta}$ is the length- m vector of
 119 locus coefficients, \mathbf{Z} is a design matrix of environment effects and other covariates, $\boldsymbol{\eta}$ is the vector
 120 of environment coefficients, ϵ is a length- n vector of residuals, and \top denotes matrix transposition.
 121 The residuals follow $\epsilon_j \sim \text{Normal}(0, \sigma_\epsilon^2)$ independently per individual j , for some σ_ϵ^2 .

122 The full model of Eq. (1), which has a coefficient for each of the m loci, is underdetermined
 123 in current datasets where $m \gg n$. The PCA and LMM models, respectively, approximate the full
 124 model fit at a single locus i :

$$\text{PCA: } \mathbf{y} = \mathbf{1}\alpha + \mathbf{x}_i\beta_i + \mathbf{U}_r\boldsymbol{\gamma}_r + \mathbf{Z}^\top\boldsymbol{\eta} + \epsilon, \quad (2)$$

$$\text{LMM: } \mathbf{y} = \mathbf{1}\alpha + \mathbf{x}_i\beta_i + \mathbf{s} + \mathbf{Z}^\top\boldsymbol{\eta} + \epsilon, \quad \mathbf{s} \sim \text{Normal}(\mathbf{0}, 2\sigma_s^2 \boldsymbol{\Phi}^T), \quad (3)$$

125 where \mathbf{x}_i is the length- n vector of genotypes at locus i only, β_i is the locus coefficient, \mathbf{U}_r is an $n \times r$
 126 matrix of PCs, $\boldsymbol{\gamma}_r$ is the length- r vector of PC coefficients, \mathbf{s} is a length- n vector of random effects,
 127 $\boldsymbol{\Phi}^T = (\varphi_{jk}^T)$ is the $n \times n$ kinship matrix conditioned on the ancestral population T , and σ_s^2 is a
 128 variance factor (do not confuse the ancestral population superscript T with the matrix transposition
 129 symbol \top). Both models condition the regression of the focal locus i on an approximation of the
 130 total polygenic effect $\mathbf{X}^\top\boldsymbol{\beta}$ with the same covariance structure, which is parametrized by the kinship
 131 matrix. Under the kinship model, genotypes are random variables obeying

$$132 \quad \mathbb{E}[\mathbf{x}_i|T] = 2p_i^T \mathbf{1}, \quad \text{Cov}(\mathbf{x}_i|T) = 4p_i^T(1 - p_i^T)\boldsymbol{\Phi}^T, \quad (4)$$

133 where p_i^T is the ancestral allele frequency of locus i [1, 68–70]. Assuming independent loci, the
 134 covariance of the polygenic effect is

$$\text{Cov}(\mathbf{X}^\top\boldsymbol{\beta}) = 2\sigma_s^2 \boldsymbol{\Phi}^T, \quad \sigma_s^2 = \sum_{i=1}^m 2p_i^T(1 - p_i^T)\beta_i^2,$$

135 which is readily modeled by the LMM random effect \mathbf{s} . (The difference in mean is absorbed by
 136 the intercept.) Alternatively, consider the eigendecomposition of the kinship matrix $\boldsymbol{\Phi}^T = \mathbf{U}\boldsymbol{\Lambda}\mathbf{U}^\top$
 137 where \mathbf{U} is the $n \times n$ eigenvector matrix and $\boldsymbol{\Lambda}$ is the $n \times n$ diagonal matrix of eigenvalues. The

138 random effect can be written as

$$\mathbf{s} = \mathbf{U}\boldsymbol{\gamma}_{\text{LMM}}, \quad \boldsymbol{\gamma}_{\text{LMM}} \sim \text{Normal}(\mathbf{0}, 2\sigma_s^2 \boldsymbol{\Lambda}),$$

139 which follows from the affine transformation property of multivariate normal distributions. There-
140 fore, the PCA term $\mathbf{U}_r \boldsymbol{\gamma}_r$ can be derived from the above equation under the additional assumption
141 that the kinship matrix has dimensionality r and the coefficients $\boldsymbol{\gamma}_r$ are fit without constraints. In
142 contrast, the LMM uses all eigenvectors, while effectively shrinking their coefficients $\boldsymbol{\gamma}_{\text{LMM}}$ as all
143 random effects models do, although these parameters are marginalized [1, 18, 47]. PCA has more
144 parameters than LMM, so it may overfit more: ignoring the shared terms in Eqs. (2) and (3), PCA
145 fits r parameters (length of $\boldsymbol{\gamma}$), whereas LMMs fit only one (σ_s^2).

146 In practice, the kinship matrix used for PCA and LMM is estimated with variations of a method-
147 of-moments formula applied to standardized genotypes \mathbf{X}_S , which is derived from Eq. (4):

$$148 \quad \mathbf{X}_S = \left(\frac{x_{ij} - 2\hat{p}_i^T}{\sqrt{4\hat{p}_i^T(1-\hat{p}_i^T)}} \right), \quad \hat{\boldsymbol{\Phi}}^T = \frac{1}{m} \mathbf{X}_S^T \mathbf{X}_S, \quad (5)$$

149 where the unknown p_i^T is estimated by $\hat{p}_i^T = \frac{1}{2n} \sum_{j=1}^n x_{ij}$ [5, 30, 34, 35, 38, 42, 44, 46, 54]. However,
150 this kinship estimator has a complex bias that differs for every individual pair, which arises due
151 to the use of this estimated \hat{p}_i^T [31, 71]. Nevertheless, in PCA and LMM these biased estimates
152 perform as well as unbiased ones [72].

153 We selected fast and robust software implementing the basic PCA and LMM models. PCA
154 association was performed with `plink2` [73]. The quantitative trait association model is a linear
155 regression with covariates, evaluated using the t-test. PCs were calculated with `plink2`, which equal
156 the top eigenvectors of Eq. (5) after removing loci with minor allele frequency MAF < 0.1.

157 LMM association was performed using GCTA [34, 42]. Its kinship estimator equals Eq. (5).
158 PCs were calculated using GCTA from its kinship estimate. Association significance is evaluated
159 with a score test. GCTA with large numbers of PCs (small simulation only) had convergence and
160 singularity errors in some replicates, which were treated as missing data.

161 **2.2 Simulations**

162 Every simulation was replicated 50 times, drawing anew all genotypes (except for real datasets)
163 and traits. Below we use the notation f_A^B for the inbreeding coefficient of a subpopulation A from
164 another subpopulation B ancestral to A . In the special case of the *total* inbreeding of A , f_A^T , T is
165 an overall ancestral population (ancestral to every individual under consideration, such as the most
166 recent common ancestor (MRCA) population).

167 **2.2.1 Genotype simulation from the admixture model**

168 The basic admixture model is as described previously [31] and is implemented in the R package
169 **bnpstd**. Large and Family have $n = 1,000$ individuals, while Small has $n = 100$. The number of loci
170 is $m = 100,000$. Individuals are admixed from $K = 10$ intermediate subpopulations, or ancestries.
171 Each subpopulation S_u ($u \in \{1, \dots, K\}$) is at coordinate u and has an inbreeding coefficient $f_{S_u}^T = u\tau$
172 for some τ . Ancestry proportions q_{ju} for individual j and S_u arise from a random walk with spread
173 σ on the 1D geography, and τ and σ are fit to give $F_{ST} = 0.1$ and mean kinship $\bar{\theta}^T = 0.5F_{ST}$ for the
174 admixed individuals [31]. Random ancestral allele frequencies p_i^T , subpopulation allele frequencies
175 $p_i^{S_u}$, individual-specific allele frequencies π_{ij} , and genotypes x_{ij} are drawn from this hierarchical
176 model:

$$\begin{aligned} p_i^T &\sim \text{Uniform}(0.01, 0.5), \\ p_i^{S_u} | p_i^T &\sim \text{Beta}\left(p_i^T \left(\frac{1}{f_{S_u}^T} - 1\right), (1 - p_i^T) \left(\frac{1}{f_{S_u}^T} - 1\right)\right), \\ \pi_{ij} &= \sum_{u=1}^K q_{ju} p_i^{S_u}, \\ x_{ij} | \pi_{ij} &\sim \text{Binomial}(2, \pi_{ij}), \end{aligned}$$

177 where this Beta is the Balding-Nichols distribution [74] with mean p_i^T and variance $p_i^T (1 - p_i^T) f_{S_u}^T$.
178 Fixed loci (i where $x_{ij} = 0$ for all j , or $x_{ij} = 2$ for all j) are drawn again from the model, starting
179 from p_i^T , iterating until no loci are fixed. Each replicate draws a genotypes starting from p_i^T .
180 As a brief aside, we prove that global ancestry proportions as covariates is equivalent in expec-

tation to using PCs under the admixture model. Note that the latent space of \mathbf{X} , given by (π_{ij}) , has K dimensions (number of columns of $\mathbf{Q} = (q_{ju})$), so the top K PCs span this space. Since associations include an intercept term ($\mathbf{1}\alpha$ in Eq. (2)), estimated PCs are orthogonal to $\mathbf{1}$ (note $\hat{\Phi}^T \mathbf{1} = \mathbf{0}$ because $\mathbf{X}_S \mathbf{1} = \mathbf{0}$), and the sum of rows of \mathbf{Q} sums to one, then only $K - 1$ PCs (plus intercept) are needed to span the latent space of this admixture model.

2.2.2 Genotype simulation from random admixed families

We simulated a pedigree with admixed founders, no close relative pairings, assortative mating based on a 1D geography (to preserve admixture structure), random family sizes, and arbitrary numbers of generations (20 here). This simulation is implemented in the R package `simfam`. Generations are drawn iteratively. Generation 1 has $n = 1000$ individuals from the above admixture simulation ordered by their 1D geography. Local kinship measures pedigree relatedness; in the first generation, everybody is locally unrelated and outbred. Individuals are randomly assigned sex. In the next generation, individuals are paired iteratively, removing random males from the pool of available males and pairing them with the nearest available female with local kinship $< 1/4^3$ (stay unpaired if there are no matches), until there are no more available males or females. Let $n = 1000$ be the desired population size, $n_m = 1$ the minimum number of children and n_f the number of families (paired parents) in the current generation, then the number of additional children (beyond the minimum) is drawn from $\text{Poisson}(n/n_f - n_m)$. Let δ be the difference between desired and current population sizes. If $\delta > 0$, then δ random families are incremented by 1. If $\delta < 0$, then $|\delta|$ random families with at least $n_m + 1$ children are decremented by 1. If $|\delta|$ exceeds the number of families, all families are incremented or decremented as needed and the process is iterated. Children are assigned sex randomly, and are reordered by the average coordinate of their parents. Children draw alleles from their parents independently per locus. A new random pedigree is drawn for each replicate, as well as new founder genotypes from the admixture model.

205 **2.2.3 Genotype simulation from a tree model**

206 This model draws subpopulations allele frequencies from a hierarchical model parametrized by a
 207 tree, which is also implemented in `bnpssd` and relies on `ape` for general tree data structures and
 208 methods [75]. The ancestral population T is the root, and each node is a subpopulation S_w indexed
 209 arbitrarily. Each edge between S_w and its parent population P_w has an inbreeding coefficient $f_{S_w}^{P_w}$.
 210 p_i^T are drawn from a given distribution (constructed to mimic each real dataset in Appendix A).
 211 Given the allele frequencies $p_i^{P_w}$ of the parent population, S_w 's allele frequencies are drawn from:

$$p_i^{S_w} | p_i^{P_w} \sim \text{Beta} \left(p_i^{P_w} \left(\frac{1}{f_{S_w}^{P_w}} - 1 \right), (1 - p_i^{P_w}) \left(\frac{1}{f_{S_w}^{P_w}} - 1 \right) \right).$$

212 Individuals j in S_w draw genotypes from its allele frequency: $x_{ij} | p_i^{S_w} \sim \text{Binomial}(2, p_i^{S_w})$. Loci
 213 with MAF < 0.01 are drawn again starting from the p_i^T distribution, iterating until no such loci
 214 remain.

215 **2.2.4 Fitting tree to real data**

216 We developed new methods to fit trees to real data based on unbiased kinship estimates from
 217 `popkin`, implemented in `bnpssd`. A tree with given inbreeding edges $f_{S_w}^{P_w}$ gives rise to a coancestry
 218 matrix ϑ_{uv}^T for a subpopulation pair (S_u, S_v) , and the goal is to recover the inbreeding edges from
 219 coancestry estimates. Coancestry values are total inbreeding coefficients of the MRCA population
 220 of each subpopulation pair. Therefore, we calculate $f_{S_w}^T$ for every S_w recursively from the root as
 221 follows. Nodes with parent $P_w = T$ are already as desired. Given $f_{P_w}^T$, the desired $f_{S_w}^T$ is calculated
 222 via the additive edge δ_w [31]:

$$223 \quad f_{S_w}^T = f_{P_w}^T + \delta_w, \quad \delta_w = f_{S_w}^{P_w} (1 - f_{P_w}^T). \quad (6)$$

224 These $\delta_w \geq 0$ because $0 \leq f_{S_w}^{P_w}, f_{P_w}^T \leq 1$ for every w . Inbreeding edges can be recovered from additive
225 edges: $f_{S_w}^{P_w} = \delta_w / (1 - f_{P_w}^T)$. Overall, coancestry values are sums of δ_w over common ancestor nodes,

226

$$\vartheta_{uv}^T = \sum_w \delta_w I_w(u, v), \quad (7)$$

227 where the sum includes all w , and $I_w(u, v)$ equals 1 if S_w is a common ancestor of S_u, S_v , 0 otherwise.

228 Note that $I_w(u, v)$ reflects tree topology and δ_w edge values.

229 To estimate population-level coancestry, first kinship ($\hat{\varphi}_{jk}^T$) is estimated using `popkin` [31]. In-
230 dividual coancestry ($\hat{\theta}_{jk}^T$) is estimated from kinship using

231

$$\hat{\theta}_{jk}^T = \begin{cases} \hat{\varphi}_{jk}^T & \text{if } k \neq j, \\ \hat{f}_j^T = 2\hat{\varphi}_{jj}^T - 1 & \text{if } k = j. \end{cases} \quad (8)$$

232 Lastly, coancestry $\hat{\vartheta}_{uv}^T$ between subpopulations are averages of individual coancestry values:

$$\hat{\vartheta}_{uv}^T = \frac{1}{|S_u||S_v|} \sum_{j \in S_u} \sum_{k \in S_v} \hat{\theta}_{jk}^T.$$

233 Topology is estimated with hierarchical clustering using the weighted pair group method with
234 arithmetic mean [76], with distance function $d(S_u, S_v) = \max \left\{ \hat{\vartheta}_{uv}^T \right\} - \hat{\vartheta}_{uv}^T$, which succeeds due to
235 the monotonic relationship between node depth and coancestry (Eq. (7)). This algorithm recovers
236 the true topology from the true coancestry values, and performs well for estimates from genotypes.

237 To estimate tree edge lengths, first δ_w are estimated from $\hat{\vartheta}_{uv}^T$ and the topology using Eq. (7) and
238 non-negative least squares linear regression [77] (implemented in `nnls` [78]) to yield non-negative
239 δ_w , and $f_{S_w}^{P_w}$ are calculated from δ_w by reversing Eq. (6). To account for small biases in coancestry
240 estimation, an intercept term δ_0 is included ($I_0(u, v) = 1$ for all u, v), and when converting δ_w to
241 $f_{S_w}^{P_w}$, δ_0 is treated as an additional edge to the root, but is ignored when drawing allele frequencies
242 from the tree.

243 **2.2.5 Trait Simulation**

244 Traits are simulated from the quantitative trait model of Eq. (1), with novel bias corrections for
245 simulating the desired heritability from real data relying on the unbiased kinship estimator `popkin`
246 [31]. This simulation is implemented in the R package `simtrait`. All simulations have a fixed
247 narrow-sense heritability of h^2 , a variance proportion due to environment effects σ_η^2 , and residuals
248 are drawn from $\epsilon_j \sim \text{Normal}(0, \sigma_\epsilon^2)$ with $\sigma_\epsilon^2 = 1 - h^2 - \sigma_\eta^2$. The number of causal loci m_1 , which
249 determines the average coefficient size, is chosen with the formula $m_1 = \text{round}(nh^2/8)$, which
250 empirically balances power well with varying n and h^2 . The set of causal loci C is drawn anew for
251 each replicate, from loci with MAF ≥ 0.01 to avoid rare causal variants (inappropriate for PCA
252 and LMM). Letting $v_i^T = p_i^T (1 - p_i^T)$, the effect size of locus i equals $2v_i^T \beta_i^2$, its contribution of the
253 trait variance [79]. Under the *fixed effect sizes* (FES) model, initial causal coefficients are

$$\beta_i = \frac{1}{\sqrt{2v_i^T}}$$

254 for known p_i^T ; otherwise v_i^T is replaced by the unbiased estimator [31] $\hat{v}_i^T = \hat{p}_i^T (1 - \hat{p}_i^T) / (1 - \bar{\varphi}^T)$,
255 where $\bar{\varphi}^T$ is the mean kinship estimated with `popkin`. Each causal locus is multiplied by -1 with
256 probability 0.5. Alternatively, under the *random coefficients* (RC) model, initial causal coefficients
257 are drawn independently from $\beta_i \sim \text{Normal}(0, 1)$. For both models, the initial genetic variance is
258 $\sigma_0^2 = \sum_{i \in C} 2v_i^T \beta_i^2$, replacing v_i^T with \hat{v}_i^T for unknown p_i^T (so σ_0^2 is an unbiased estimate), so we
259 multiply every initial β_i by $\frac{h}{\sigma_0}$ to have the desired heritability. Lastly, for known p_i^T , the intercept
260 coefficient is $\alpha = -\sum_{i \in C} 2p_i^T \beta_i$. When p_i^T are unknown, \hat{p}_i^T should not replace p_i^T since that distorts
261 the trait covariance (for the same reason the standard kinship estimator in Eq. (5) is biased), which
262 is avoided with

$$\alpha = -\frac{2}{m_1} \left(\sum_{i \in C} \hat{p}_i^T \right) \left(\sum_{i \in C} \beta_i \right).$$

263 Simulations optionally included multiple environment group effects, similarly to previous models
264 [18, 33], as follows. Each independent environment i has predefined groups, and each group g has
265 random coefficients drawn independent from $\eta_{gi} \sim \text{Normal}(0, \sigma_{\eta i}^2)$ where $\sigma_{\eta i}^2$ is a specified variance

266 proportion for environment i . \mathbf{Z} has individuals along columns and environment-groups along rows,
267 and it contains indicator variables: 1 if the individual belongs to the environment-group, 0 otherwise.

268 We performed trait simulations with the following variance parameters (Table 2): *high heritability*
269 used $h^2 = 0.8$ and no environment effects; *low heritability* used $h^2 = 0.3$ and no environment
270 effects; lastly, *environment* used $h^2 = 0.3$, $\sigma_{\eta_1}^2 = 0.3$, $\sigma_{\eta_2}^2 = 0.2$ (total $\sigma_{\eta}^2 = \sigma_{\eta_1}^2 + \sigma_{\eta_2}^2 = 0.5$). For
271 real genotype datasets, the groups are the subpopulation (environment 1) and sub-subpopulation
272 (environment 2) labels given (see next subsection). For simulated genotypes, we created these labels
273 by grouping by the index j (geographical coordinate) of each simulated individual, assigning group
274 $g = \text{ceiling}(jk_i/n)$ where k_i is the number of groups in environment i , and we selected $k_1 = 5$ and
275 $k_2 = 25$ to mimic the number of groups in each level of 1000 Genomes (Table 3).

Table 2: **Variance parameters of trait simulations.**

Trait variance type	h^2	σ_{η}^2	σ_{ϵ}^2
High heritability	0.8	0.0	0.2
Low heritability	0.3	0.0	0.7
Environment	0.3	0.5	0.2

Table 3: **Features of simulated and real human genotype datasets.**

Dataset	Type	Loci (m)	Ind. (n)	Subpops. ^a (K)	Causal loci ^b (m_1)	F_{ST} ^c
Admix. Large sim.	Admix.	100,000	1000	10	100	0.1
Admix. Small sim.	Admix.	100,000	100	10	10	0.1
Admix. Family sim.	Admix.+Pedig.	100,000	1000	10	100	0.1
Human Origins	Real	190,394	2922	11-243	292	0.28
HGDP	Real	771,322	929	7-54	93	0.28
1000 Genomes	Real	1,111,266	2504	5-26	250	0.22
Human Origins sim.	Tree	190,394	2922	243	292	0.23
HGDP sim.	Tree	771,322	929	54	93	0.25
1000 Genomes sim.	Tree	1,111,266	2504	26	250	0.21

^aFor admixed family, ignores dimensionality of 20 generation pedigree structure. For real datasets, lower range is continental subpopulations, upper range is number of fine-grained subpopulations.

^b $m_1 = \text{round}(nh^2/8)$ to balance power across datasets, shown for $h^2 = 0.8$ only.

^cModel parameter for simulations, estimated value on real datasets.

276 **2.3 Real human genotype datasets**

277 The three datasets were processed as before [71] (summarized below), except with an additional filter
278 so loci are in approximate linkage equilibrium and rare variants are removed. All processing was
279 performed with `plink2` [73], and analysis was uniquely enabled by the R packages `BEDMatrix` [80]
280 and `genio`. Each dataset groups individuals in a two-level hierarchy: continental and fine-grained
281 subpopulations. Final dataset sizes are in Table 3.

282 We obtained the full (including non-public) Human Origins by contacting the authors and
283 agreeing to their usage restrictions. The Pacific data [64] was obtained separately from the rest [62,
284 63], and datasets were merged using the intersection of loci. We removed ancient individuals, and
285 individuals from singleton and non-native subpopulations. Non-autosomal loci were removed. Our
286 analysis of the whole-genome sequencing (WGS) version of HGDP [60] was restricted to autosomal
287 biallelic SNP loci with filter “PASS”. Our analysis of the high-coverage NYGC version of 1000
288 Genomes [81] was restricted to autosomal biallelic SNP loci with filter “PASS”.

289 Since our evaluations assume uncorrelated loci, we filtered each dataset with `plink2` using
290 parameters “`--indep-pairwise 1000kb 0.3`”, which iteratively removes loci that have a greater
291 than 0.3 squared correlation coefficient with another locus that is within 1000kb, stopping until no
292 such loci remain. Since all real datasets have numerous rare variants, while PCA and LMM are not
293 able to detect associations involving rare variants, we removed all loci with $\text{MAF} < 0.01$. Lastly,
294 only HGDP had loci with over 10% missingness removed, as they were otherwise 17% of remaining
295 loci (for Human Origins and 1000 Genomes they were under 1% of loci so they were not removed).
296 Kinship dimensionality and eigenvalues were calculated from `popkin` kinship estimates. Eigenvalues
297 were assigned p-values with `twstats` of the Eigensoft package [7], and dimensionality was estimated
298 as the largest number of consecutive eigenvalue from the start that all satisfy $p < 0.01$ (p-values
299 did not increase monotonically). For the evaluation with close relatives removed, each dataset was
300 filtered with `plink2` with option “`--king-cutoff`” with cutoff $0.02209709 (= 2^{-11/2})$ for removing
301 up to 4th degree relatives using KING-robust [82], and $\text{MAF} < 0.01$ filter is reapplied (Table S1).

302 **2.4 Evaluation of performance**

303 All approaches are evaluated in two orthogonal dimensions: SRMSD_p quantifies p-value uniformity,
 304 and AUC_{PR} measures causal locus classification performance and reflects power while ranking mis-
 305 calibrated models fairly. These measures are more robust alternatives to previous measures from
 306 the literature (see Appendix B), and are implemented in **simtrait**.

307 P-values for continuous test statistics have a uniform distribution when the null hypothesis
 308 holds, a crucial assumption for type I error and FDR control [83, 84]. We use the Signed Root
 309 Mean Square Deviation (SRMSD_p) to measure the difference between the observed null p-value
 310 quantiles and the expected uniform quantiles:

$$\text{SRMSD}_p = \text{sgn}(u_{\text{median}} - p_{\text{median}}) \sqrt{\frac{1}{m_0} \sum_{i=1}^{m_0} (u_i - p_{(i)})^2},$$

311 where $m_0 = m - m_1$ is the number of null (non-causal) loci, here i indexes null loci only, $p_{(i)}$ is
 312 the i th ordered null p-value, $u_i = (i - 0.5)/m_0$ is its expectation, p_{median} is the median observed
 313 null p-value, $u_{\text{median}} = \frac{1}{2}$ is its expectation, and sgn is the sign function (1 if $u_{\text{median}} \geq p_{\text{median}}$,
 314 -1 otherwise). Thus, $\text{SRMSD}_p = 0$ corresponds to calibrated p-values, $\text{SRMSD}_p > 0$ indicate anti-
 315 conservative p-values, and $\text{SRMSD}_p < 0$ are conservative p-values. The maximum SRMSD_p is
 316 achieved when all p-values are zero (the limit of anti-conservative p-values), which for infinite loci
 317 approaches

$$\text{SRMSD}_p \rightarrow \sqrt{\int_0^1 u^2 du} = \frac{1}{\sqrt{3}} \approx 0.577.$$

318 The same value (with negative sign) occurs for all p-values of 1.

319 Precision and recall are standard performance measures for binary classifiers that do not require
 320 calibrated p-values [85]. Given the total numbers of true positives (TP), false positives (FP) and
 321 false negatives (FN) at some threshold or parameter t , precision and recall are

$$\begin{aligned} \text{Precision}(t) &= \frac{\text{TP}(t)}{\text{TP}(t) + \text{FP}(t)}, \\ \text{Recall}(t) &= \frac{\text{TP}(t)}{\text{TP}(t) + \text{FN}(t)}. \end{aligned}$$

322 Precision and Recall trace a curve as t is varied, and the area under this curve is AUC_{PR} . We use the
323 R package **PRROC** to integrate the correct non-linear piecewise function when interpolating between
324 points. A model obtains the maximum $AUC_{PR} = 1$ if there is a t that classifies all loci perfectly. In
325 contrast, the worst models, which classify at random, have an expected precision ($= AUC_{PR}$) equal
326 to the overall proportion of causal loci: $\frac{m_1}{m}$.

327 3 Results

328 3.1 Overview of evaluations

329 We use three real genotype datasets and simulated genotypes from six population structure scenarios
330 to cover various features of interest (Table 3). We introduce them in sets of three, as they appear
331 in the rest of our results. Population kinship matrices, which combine population and family
332 relatedness, are estimated without bias using **popkin** [31] (Fig. 1). The first set of three simulated
333 genotypes are based on an admixture model with 10 ancestries (Fig. 1A) [14, 31, 86]. The “large”
334 version (1000 individuals) illustrates asymptotic performance, while the “small” simulation (100
335 individuals) illustrates model overfitting. The “family” simulation has admixed founders and draws
336 a 20-generation random pedigree with assortative mating, resulting in a complex joint family and
337 ancestry structure in the last generation (Fig. 1B). The second set of three are the real human
338 datasets representing global human diversity: Human Origins (Fig. 1D), HGDP (Fig. 1G), and
339 1000 Genomes (Fig. 1J), which are enriched for small minor allele frequencies even after $MAF < 1\%$
340 filter (Fig. 1C). Last are tree simulations (Fig. 1F,I,L) fit to the kinship (Fig. 1E,H,K) and MAF
341 (Fig. 1C) of each real human dataset, which by design do not have family structure.

342 All traits in this work are simulated. We repeated all evaluations on two additive quantitative
343 trait models, *fixed effect sizes* (FES) and *random coefficients* (RC), which differ in how causal coef-
344 ficients are constructed. The FES model captures the rough inverse relationship between coefficient
345 and minor allele frequency that arises under strong negative and balancing selection and has been
346 observed in numerous diseases and other traits [50, 65–67], so it is the focus of our results. The
347 RC model draws coefficients independent of allele frequency, corresponding to neutral traits [50,

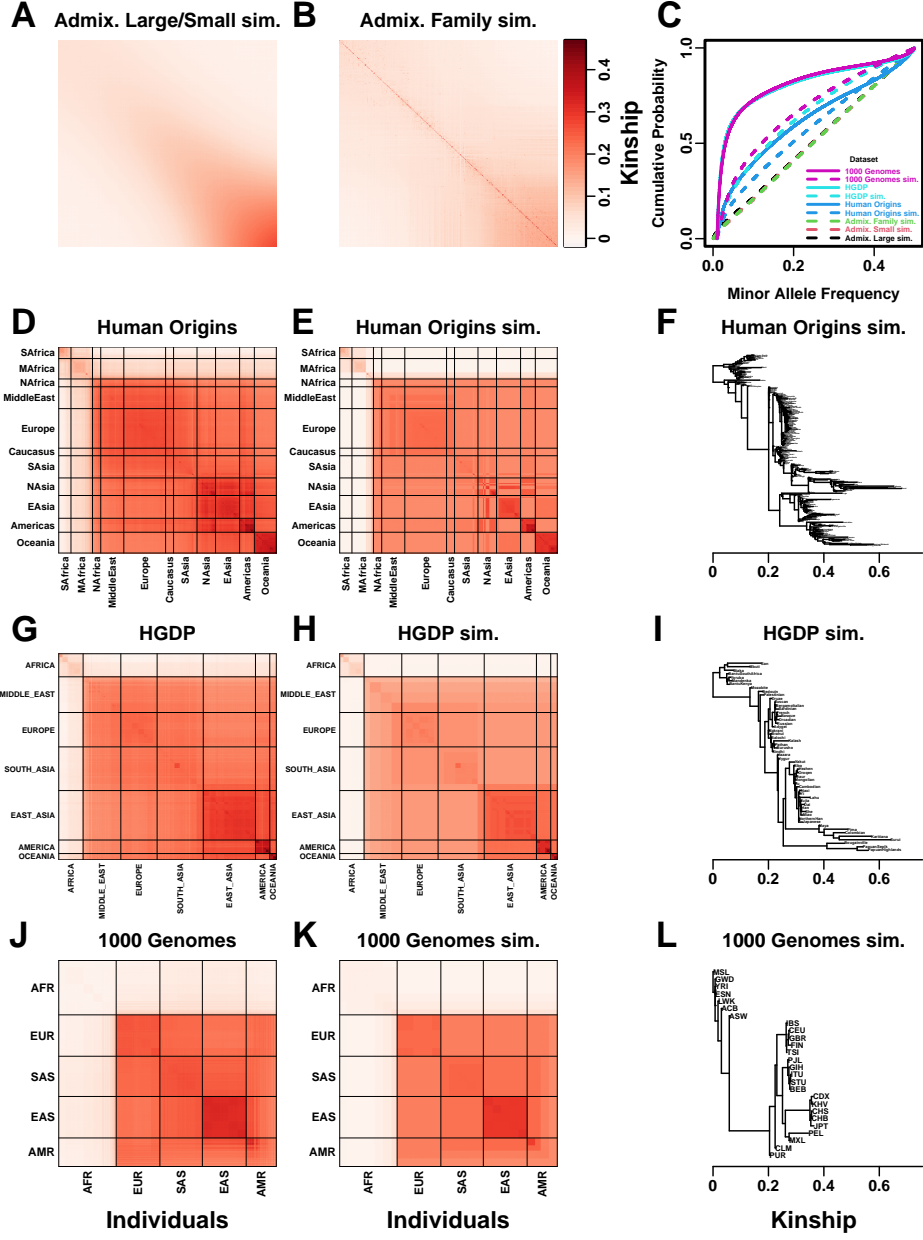


Figure 1: Population structures of simulated and real human genotype datasets. First two columns are population kinship matrices as heatmaps: individuals along x- and y-axis, kinship as color. Diagonal shows inbreeding values. **A.** Admixture scenario for both Large and Small simulations. **B.** Last generation of 20-generation admixed family, shows larger kinship values near diagonal corresponding to siblings, first cousins, etc. **C.** Minor allele frequency (MAF) distributions. Real datasets and tree simulations had $\text{MAF} \geq 0.01$ filter. **D.** Human Origins is an array dataset of a large diversity of global populations. **G.** Human Genome Diversity Panel (HGDP) is a WGS dataset from global native populations. **J.** 1000 Genomes Project is a WGS dataset of global cosmopolitan populations. **F,I,L.** Trees between subpopulations fit to real data. **E,H,K.** Simulations from trees fit to the real data recapitulate subpopulation structure.

³⁴⁸ 67], which results in a wider effect size distribution that reduces association power and effective
³⁴⁹ polygenicity compared to FES.

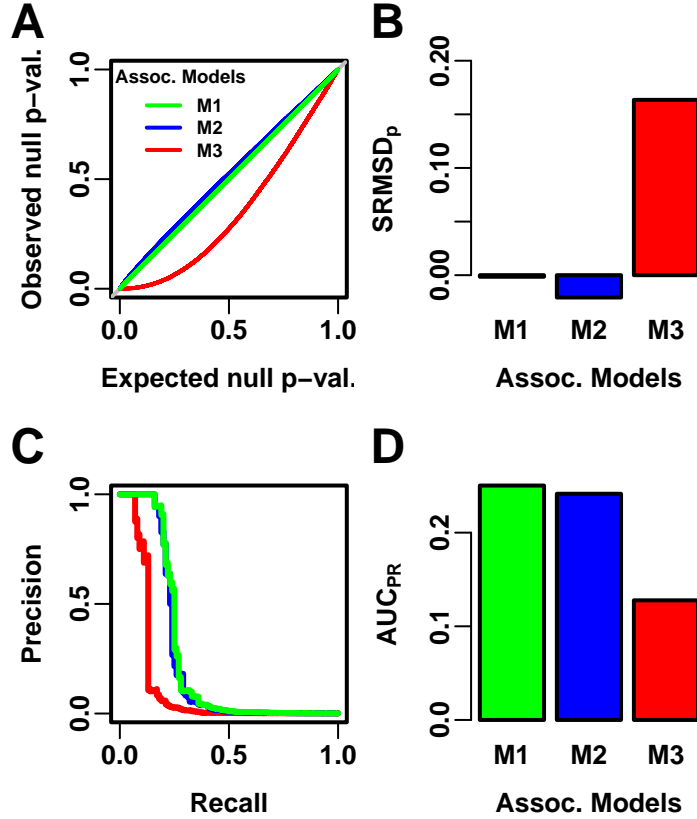


Figure 2: **Illustration of evaluation measures.** Three archetypal models illustrate our complementary measures: M1 is ideal, M2 overfits slightly, M3 is naive. **A.** QQ plot of p-values of “null” (non-causal) loci. M1 has desired uniform p-values, M2/M3 are miscalibrated. **B.** SRMSD_p (p-value Signed Root Mean Square Deviation) measures signed distance between observed and expected null p-values (closer to zero is better). **C.** Precision and Recall (PR) measure causal locus classification performance (higher is better). **D.** AUC_{PR} (Area Under the PR Curve) reflects power (higher is better).

³⁵⁰ We evaluate using two complementary measures: (1) SRMSD_p (p-value signed root mean square
³⁵¹ deviation) measures p-value calibration (closer to zero is better), and (2) AUC_{PR} (precision-recall
³⁵² area under the curve) measures causal locus classification performance (higher is better; Fig. 2).
³⁵³ SRMSD_p is a more robust alternative to the common inflation factor λ and type I error control
³⁵⁴ measures; there is a correspondence between λ and SRMSD_p, with SRMSD_p > 0.01 giving $\lambda > 1.06$
³⁵⁵ (Fig. S1) and thus evidence of miscalibration close to the rule of thumb of $\lambda > 1.05$ [23]. AUC_{PR}

356 has been used to evaluate association models [87], and reflects statistical power while being robust
 357 to miscalibrated models (Appendix B).

358 Both PCA and LMM are evaluated in each replicate dataset including a number of PCs r
 359 between 0 and 90 as fixed covariates. In terms of p-value calibration, for PCA the best number of
 360 PCs r (minimizing mean $|\text{SRMSD}_p|$ over replicates) is typically large across all datasets (Table 4),
 361 although much smaller r values often performed as well (shown in following sections). Most cases

Table 4: Overview of PCA and LMM evaluations for high heritability simulations

Dataset	Metric	Trait ^a	LMM $r = 0$ vs best r			Best r^c	PCA vs LMM $r = 0$		
			Cal. ^b	Best r^c	P-value ^d		Cal. ^b	P-value ^d	Best model ^e
Admix. Large sim.	$ \text{SRMSD}_p $	FES	True	0	1	12	True	0.036	Tie
Admix. Small sim.	$ \text{SRMSD}_p $	FES	True	0	1	4	True	0.055	Tie
Admix. Family sim.	$ \text{SRMSD}_p $	FES	True	0	1	90	False	3.9e-10*	LMM
Human Origins	$ \text{SRMSD}_p $	FES	True	0	1	89	False	3.9e-10*	LMM
HGDP	$ \text{SRMSD}_p $	FES	True	0	1	87	True	4.4e-10*	LMM
1000 Genomes	$ \text{SRMSD}_p $	FES	True	0	1	90	False	3.9e-10*	LMM
Human Origins sim.	$ \text{SRMSD}_p $	FES	True	0	1	88	True	0.017	Tie
HGDP sim.	$ \text{SRMSD}_p $	FES	True	0	1	47	True	0.046	Tie
1000 Genomes sim.	$ \text{SRMSD}_p $	FES	True	0	1	78	True	9.6e-10*	LMM
Admix. Large sim.	$ \text{SRMSD}_p $	RC	True	0	1	26	True	0.11	Tie
Admix. Small sim.	$ \text{SRMSD}_p $	RC	True	0	1	4	True	0.00097	Tie
Admix. Family sim.	$ \text{SRMSD}_p $	RC	True	0	1	90	False	3.9e-10*	LMM
Human Origins	$ \text{SRMSD}_p $	RC	True	0	1	90	True	0.00065	Tie
HGDP	$ \text{SRMSD}_p $	RC	True	0	1	37	True	1.5e-05*	LMM
1000 Genomes	$ \text{SRMSD}_p $	RC	True	0	1	76	True	3.9e-10*	LMM
Human Origins sim.	$ \text{SRMSD}_p $	RC	True	0	1	85	True	0.14	Tie
HGDP sim.	$ \text{SRMSD}_p $	RC	True	0	1	44	True	8.8e-07*	LMM
1000 Genomes sim.	$ \text{SRMSD}_p $	RC	True	0	1	90	True	3.9e-10*	LMM
Admix. Large sim.	AUC_{PR}	FES		0	1	3		5.9e-06*	LMM
Admix. Small sim.	AUC_{PR}	FES		0	1	2		0.025	Tie
Admix. Family sim.	AUC_{PR}	FES		1	0.35	22		3.9e-10*	LMM
Human Origins	AUC_{PR}	FES		0	1	34		3.9e-10*	LMM
HGDP	AUC_{PR}	FES		1	0.33	16		4.4e-10*	LMM
1000 Genomes	AUC_{PR}	FES		1	0.11	8		3.9e-10*	LMM
Human Origins sim.	AUC_{PR}	FES		0	1	36		3.9e-10*	LMM
HGDP sim.	AUC_{PR}	FES		0	1	17		1.7e-05*	LMM
1000 Genomes sim.	AUC_{PR}	FES		0	1	10		5e-10*	LMM
Admix. Large sim.	AUC_{PR}	RC		0	1	3		1.4e-05*	LMM
Admix. Small sim.	AUC_{PR}	RC		0	1	1		0.095	Tie
Admix. Family sim.	AUC_{PR}	RC		0	1	34		3.9e-10*	LMM
Human Origins	AUC_{PR}	RC		3	0.4	36		9.6e-10*	LMM
HGDP	AUC_{PR}	RC		4	0.21	16		0.013	Tie
1000 Genomes	AUC_{PR}	RC		5	0.004	9		0.00043	Tie
Human Origins sim.	AUC_{PR}	RC		0	1	37		4.1e-10*	LMM
HGDP sim.	AUC_{PR}	RC		3	0.087	17		0.0014	Tie
1000 Genomes sim.	AUC_{PR}	RC		3	0.37	10		8.5e-10*	LMM

^aFES: Fixed Effect Sizes, RC: Random Coefficients.

^bCalibrated: whether mean $|\text{SRMSD}_p| < 0.01$.

^cValue of r (number of PCs) with minimum mean $|\text{SRMSD}_p|$ or maximum mean AUC_{PR} .

^dWilcoxon paired 1-tailed test of distributions ($|\text{SRMSD}_p|$ or AUC_{PR}) between models in header. Asterisk marks significant value using Bonferroni threshold ($p < \alpha/n_{\text{tests}}$ with $\alpha = 0.01$ and $n_{\text{tests}} = 72$ is the number of tests in this table).

^eTie if no significant difference using Bonferroni threshold.

362 have a mean $|\text{SRMSD}_p| < 0.01$, whose p-values are effectively calibrated. However, PCA is often
363 miscalibrated on the family simulation and real datasets (Table 4). In contrast, for LMM, $r = 0$ (no
364 PCs) is always best, and is always calibrated. Comparing LMM with $r = 0$ to PCA with its best
365 r , LMM always has significantly smaller $|\text{SRMSD}_p|$ than PCA or is statistically tied. For AUC_{PR}
366 and PCA, the best r is always smaller than the best r for $|\text{SRMSD}_p|$, so there is often a tradeoff
367 between calibrated p-values versus classification performance. For LMM there is no tradeoff, as
368 $r = 0$ often has the best mean AUC_{PR} , and otherwise is not significantly different from the best
369 r . Lastly, LMM with $r = 0$ always has significantly greater or statistically tied AUC_{PR} than PCA
370 with its best r .

371 3.2 Evaluations in admixture simulations

372 Now we look more closely at results per dataset. The complete SRMSD_p and AUC_{PR} distributions
373 for the admixture simulations and FES traits are in Fig. 3. RC traits gave qualitatively similar
374 results (Fig. S2).

375 In the large admixture simulation, the SRMSD_p of PCA is largest when $r = 0$ (no PCs) and
376 decreases rapidly to near zero at $r = 3$, where it stays for up to $r = 90$ (Fig. 3A). Thus, PCA
377 has calibrated p-values for $r \geq 3$, smaller than the theoretical optimum for this simulation of
378 $r = K - 1 = 9$. In contrast, the SRMSD_p for LMM starts near zero for $r = 0$, but becomes negative
379 as r increases (p-values are conservative). The AUC_{PR} distribution of PCA is similarly worst at
380 $r = 0$, increases rapidly and peaks at $r = 3$, then decreases slowly for $r > 3$, while the AUC_{PR}
381 distribution for LMM starts near its maximum at $r = 0$ and decreases with r . Although the AUC_{PR}
382 distributions for LMM and PCA overlap considerably at each r , LMM with $r = 0$ has significantly
383 greater AUC_{PR} values than PCA with $r = 3$ (Table 4). However, qualitatively PCA performs nearly
384 as well as LMM in this simulation.

385 The observed robustness to large r led us to consider smaller sample sizes. A model with large
386 numbers of parameters r should overfit more as r approaches the sample size n . Rather than increase
387 r beyond 90, we reduce individuals to $n = 100$, which is small for typical association studies but
388 may occur in studies of rare diseases, pilot studies, or other constraints. To compensate for the

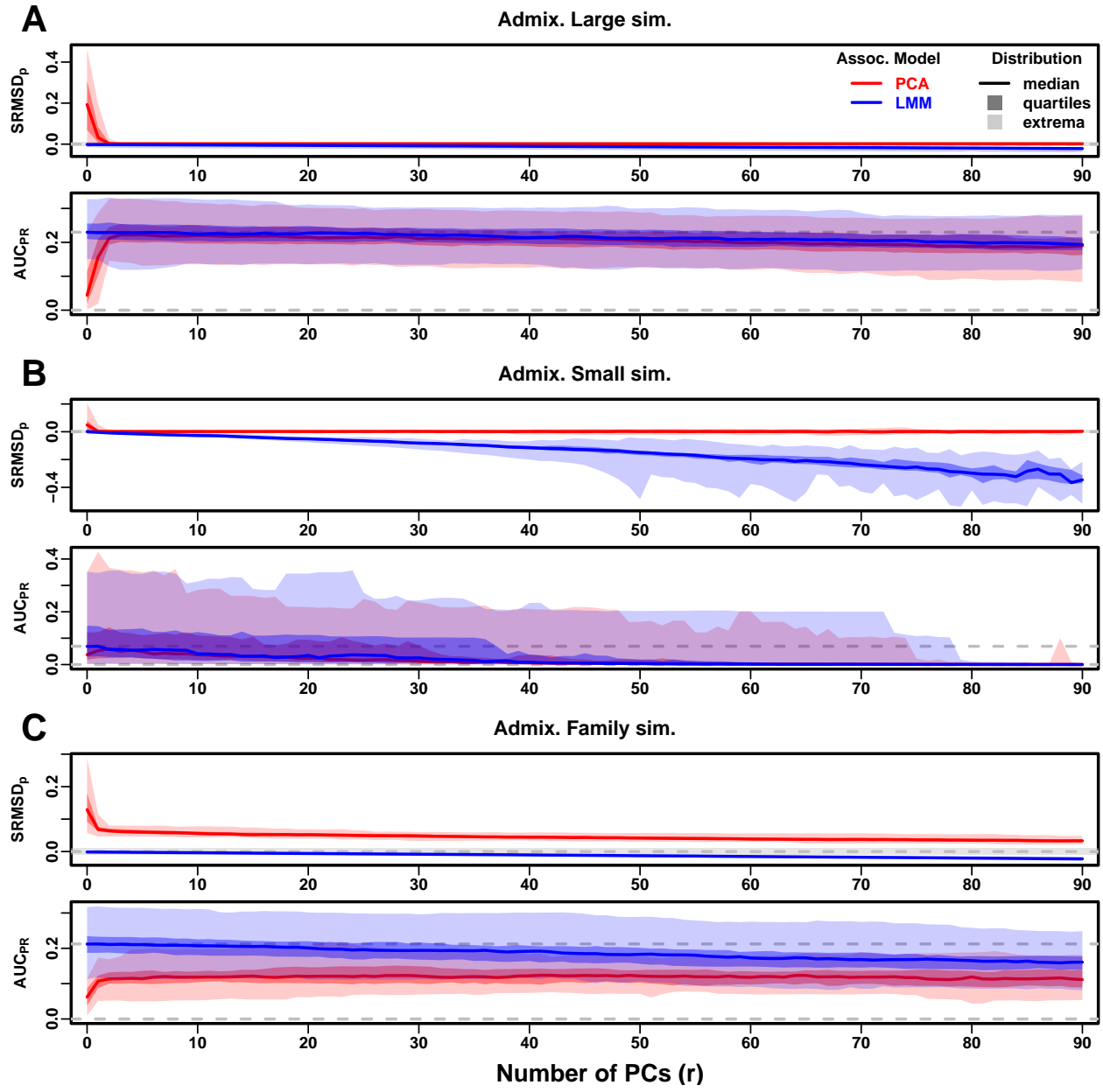


Figure 3: **Evaluations in admixture simulations.** Traits simulated from FES model with high heritability. PCA and LMM models have varying number of PCs ($r \in \{0, \dots, 90\}$ on x-axis), with the distributions (y-axis) of SRMSD_p (top subpanel) and AUC_{PR} (bottom subpanel) for 50 replicates. Best performance is zero SRMSD_p and large AUC_{PR} . Zero and maximum median AUC_{PR} values are marked with horizontal gray dashed lines, and $|\text{SRMSD}_p| < 0.01$ is marked with a light gray area. LMM performs best with $r = 0$, PCA with various r . **A.** Large simulation ($n = 1,000$ individuals). **B.** Small simulation ($n = 100$) shows overfitting for large r . **C.** Family simulation ($n = 1,000$) has admixed founders and large numbers of close relatives from a realistic random 20-generation pedigree. PCA performs poorly compared to LMM: $\text{SRMSD}_p > 0$ for all r and large AUC_{PR} gap.

389 loss of power due to reducing n , we also reduce the number of causal loci (fixed ratio $n/m_1 = 10$),
390 which increases per-locus effect sizes. We found a large decrease in performance for both models as
391 r increases, and best performance for $r = 1$ for PCA and $r = 0$ for LMM (Fig. 3B). Remarkably,
392 LMM attains much larger negative SRMSD _{p} values than in our other evaluations. LMM with $r = 0$
393 is significantly better than PCA ($r = 1$ to 4) in both measures (Table 4), but qualitatively the
394 difference is negligible.

395 The family simulation adds a 20-generation random family to our large admixture simulation.
396 Only the last generation is studied for association, which contains numerous siblings, first cousins,
397 etc., with the initial admixture structure preserved by geographically-biased mating. Our evaluation
398 reveals a sizable gap in both measures between LMM and PCA across all r (Fig. 3C). LMM again
399 performs best with $r = 0$ and achieves mean $|\text{SRMSD}_p| < 0.01$. However, PCA does not achieve
400 mean $|\text{SRMSD}_p| < 0.01$ at any r , and its best mean AUC_{PR} is considerably worse than that of
401 LMM. Thus, LMM is conclusively superior to PCA, and the only calibrated model, when there is
402 family structure.

403 3.3 Evaluations in real human genotype datasets

404 Next we repeat our evaluations with real human genotype data, which differs from our simulations in
405 allele frequency distributions and more complex population structures with greater differentiation,
406 numerous correlated subpopulations, and potential cryptic family relatedness.

407 Human Origins has the greatest number and diversity of subpopulations. The SRMSD _{p} and
408 AUC_{PR} distributions in this dataset and FES traits (Fig. 4A) most resemble those from the family
409 simulation (Fig. 3C). In particular, while LMM with $r = 0$ performed optimally (both measures)
410 and satisfies mean $|\text{SRMSD}_p| < 0.01$, PCA maintained $\text{SRMSD}_p > 0.01$ for all r and its AUC_{PR}
411 were all considerably smaller than the best AUC_{PR} of LMM.

412 HGDP has the fewest individuals among real datasets, but compared to Human Origins contains
413 more loci and low-frequency variants. Performance (Fig. 4B) again most resembled the family sim-
414 ulations. In particular, LMM with $r = 0$ achieves mean $|\text{SRMSD}_p| < 0.01$ (p-values are calibrated),
415 while PCA does not, and there is a sizable AUC_{PR} gap between LMM and PCA. Maximum AUC_{PR}

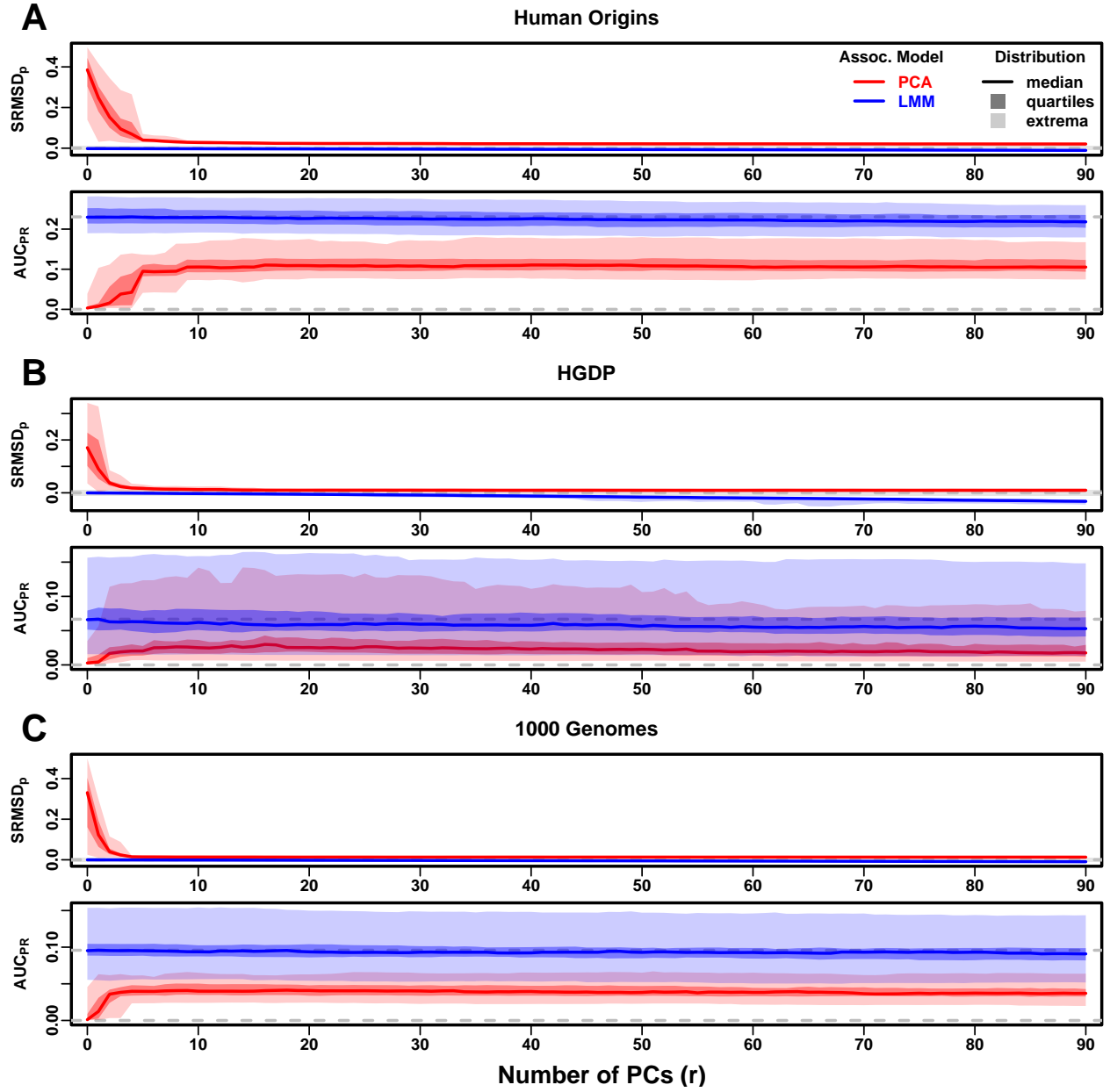


Figure 4: **Evaluations in real human genotype datasets.** Traits simulated from FES model with high heritability. Same setup as Fig. 3, see that for details. These datasets strongly favor LMM with no PCs over PCA, with distributions that most resemble the family simulation. **A.** Human Origins. **B.** Human Genome Diversity Panel (HGDP). **C.** 1000 Genomes Project.

416 values were lowest in HGDP compared to the two other real datasets.

417 1000 Genomes has the fewest subpopulations but largest number of individuals per subpopula-
418 tion. Thus, although this dataset has the simplest subpopulation structure among the real datasets,
419 we find SRMSD_p and AUC_{PR} distributions (Fig. 4C) that again most resemble our earlier family
420 simulation, with mean |SRMSD_p| < 0.01 for LMM only and large AUC_{PR} gaps between LMM and
421 PCA.

422 Our results are qualitatively different for RC traits, which had smaller AUC_{PR} gaps between
423 LMM and PCA (Fig. S3). Maximum AUC_{PR} were smaller in RC compared to FES in Human Origins
424 and 1000 Genomes, suggesting lower power for RC traits across association models. Nevertheless,
425 LMM with $r = 0$ was significantly better than PCA for all measures in the real datasets and RC
426 traits (Table 4).

427 3.4 Evaluations in tree simulations fit to human data

428 To better understand which features of the real datasets lead to the large differences in performance
429 between LMM and PCA, we carried out tree simulations. Human subpopulations are related roughly
430 by trees, which induce the strongest correlations and have numerous tips, so we fit trees to each
431 real dataset and tested if data simulated from these complex tree structures could recapitulate our
432 previous results (Fig. 1). These tree simulations also feature non-uniform ancestral allele frequency
433 distributions, which recapitulated some of the skew for smaller minor allele frequencies of the real
434 datasets (Fig. 1C). The SRMSD_p and AUC_{PR} distributions for these tree simulations (Fig. 5)
435 resembled our admixture simulation more than either the family simulation (Fig. 3) or real data
436 results (Fig. 4). Both LMM with $r = 0$ and PCA (various r) achieve mean |SRMSD_p| < 0.01
437 (Table 4). The AUC_{PR} distributions of both LMM and PCA track closely as r is varied, although
438 there is a small gap resulting in LMM ($r = 0$) besting PCA in all three simulations. The results
439 are qualitatively similar for RC traits (Fig. S4 and Table 4). Overall, these tree simulations do not
440 recapitulate the large LMM advantage over PCA observed on the real data.

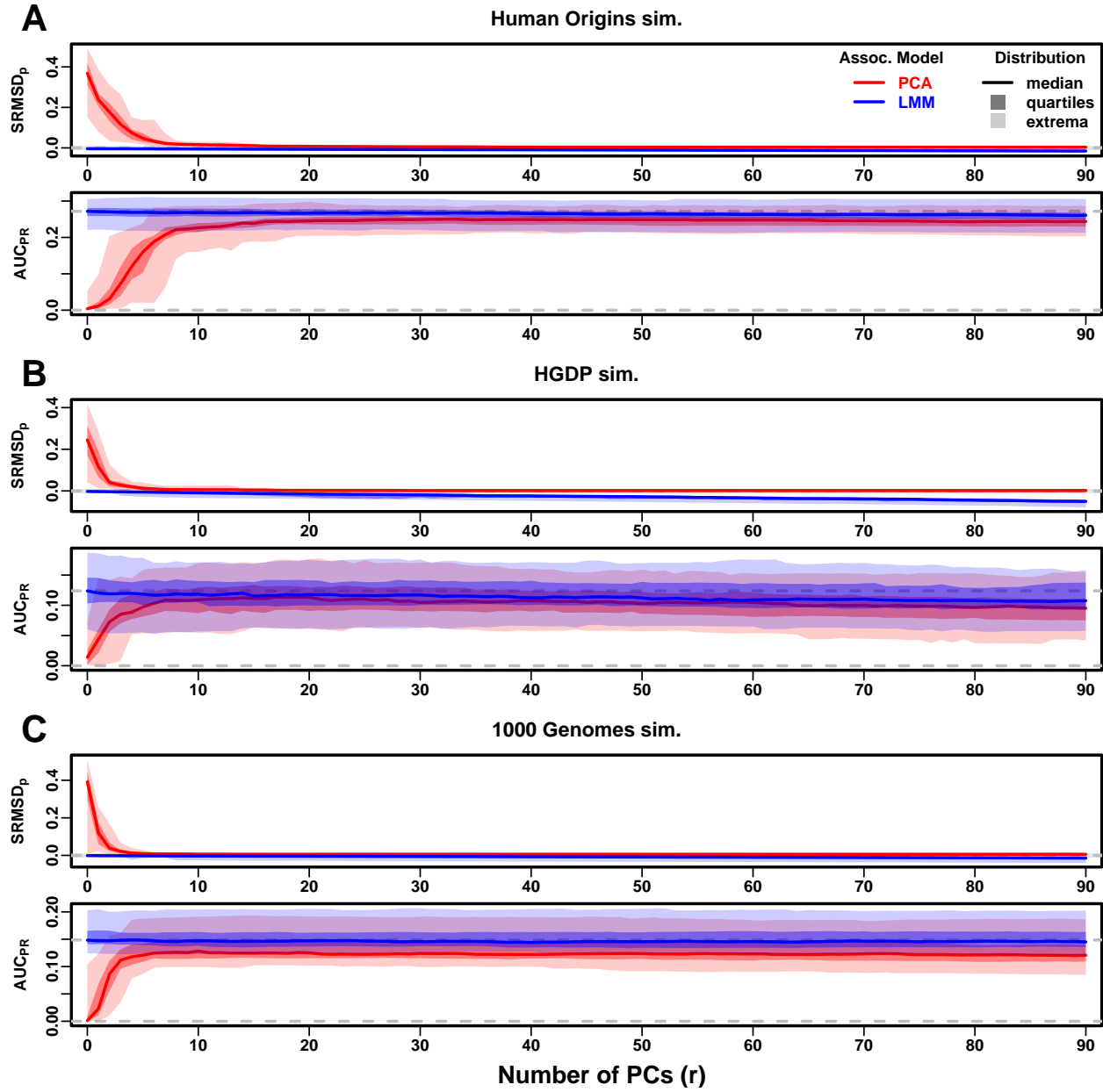


Figure 5: **Evaluations in tree simulations fit to human data.** Traits simulated from FES model with high heritability. Same setup as Fig. 3, see that for details. These tree simulations, which exclude family structure by design, do not explain the large gaps in LMM-PCA performance observed in the real data. **A.** Human Origins tree simulation. **B.** Human Genome Diversity Panel (HGDP) tree simulation. **C.** 1000 Genomes Project tree simulation.

441 **3.5 Numerous distant relatives explain poor PCA performance in real data**

442 In principle, PCA performance should be determined by the dimensionality of relatedness, since
443 PCA is a low-dimensional model whereas LMM can model high-dimensional relatedness without
444 overfitting. We used the Tracy-Widom test [7] with $p < 0.01$ to estimate dimensionality as the
445 number of significant PCs (Fig. S5A). The true dimensionality of our simulations is slightly un-
446 derestimated (Table 3), but we confirm that the family simulation has the greatest dimensionality,
447 and real datasets have greater estimates than their respective tree simulations, which confirms our
448 hypothesis to some extent. However, estimated dimensionalities do not separate real datasets from
449 tree simulations, as required to predict the observed PCA performance. Moreover, the HGDP and
450 1000 Genomes dimensionality estimates are 45 and 61, respectively, yet PCA performed poorly
451 for all $r \leq 90$ numbers of PCs (Fig. 4). The top eigenvalue explained a proportion of variance
452 proportional to F_{ST} (Table 3), but the rest of the top 10 eigenvalues show no clear differences
453 between datasets, except the small simulation had larger variances explained per eigenvalue (ex-
454 pected since it has fewer eigenvalues; Fig. S5C). Comparing cumulative variance explained versus
455 rank fraction across all eigenvalues, all datasets increase from their starting point almost linearly
456 until they reach 1, except the family simulation has much greater variance explained by mid-rank
457 eigenvalues (Fig. S5B). Overall, there is no separation between real datasets (where PCA performed
458 poorly) and tree simulations (where PCA performed relatively well) in terms of their eigenvalues or
459 dimensionality estimates.

460 Local kinship, which is recent relatedness due to family structure excluding population structure,
461 is the presumed cause of the LMM to PCA performance gap observed in real datasets but not their
462 tree simulation counterparts. Instead of inferring local kinship through increased dimensionality, as
463 attempted in the last paragraph, now we measure it directly using the KING-robust estimator [82].
464 We observe more large local kinship in the real datasets and the family simulation compared to the
465 other simulations (Fig. 6). However, for real data this distribution depends on the subpopulation
466 structure, since locally related pairs are most likely in the same subpopulation. Therefore, the
467 only comparable curve to each real dataset is their corresponding tree simulation, which matches
468 subpopulation structure. In all real datasets we identified highly related individual pairs with

469 kinship above the 4th degree relative threshold of 0.022 [82, 88]. However, these highly related pairs
 470 are vastly outnumbered by more distant pairs with evident non-zero local kinship as compared to
 471 the extreme tree simulation values.

472 To try to improve PCA performance, we followed the standard practice of removing 4th degree
 473 relatives, which reduced sample sizes between 5% and 10% (Table S1). Only $r = 0$ for LMM
 474 and $r = 20$ for PCA were tested, as these performed well in our earlier evaluation, and only
 475 FES traits were tested because they previously displayed the large PCA-LMM performance gap.
 476 LMM significantly outperforms PCA in all these cases (Wilcoxon paired 1-tailed $p < 0.01$; Fig. 7).
 477 Notably, PCA still had miscalibrated p-values in all real datasets ($|\text{SRMSD}_p| > 0.01$). Otherwise,
 478 AUC_{PR} and SRMSD_p ranges were similar here as in our earlier evaluation. Therefore, the removal
 479 of the small number of highly related individual pairs had a negligible effect in PCA performance,
 480 so the larger number of more distantly related pairs explain the poor PCA performance in the real
 481 datasets.

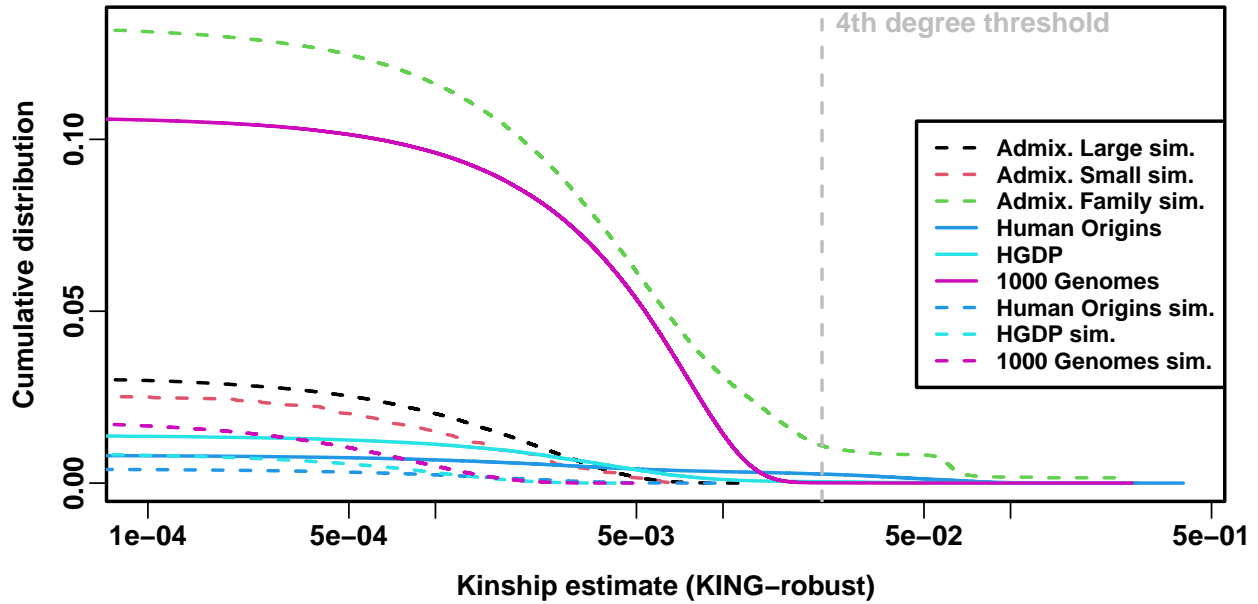


Figure 6: **Local kinship distributions.** Curves are complementary cumulative distribution of lower triangular kinship matrix (self kinship excluded) from KING-robust estimator. Note log x-axis; negative estimates are counted but not shown. Most values are below 4th degree relative threshold. Each real dataset has a greater cumulative than its tree simulations.

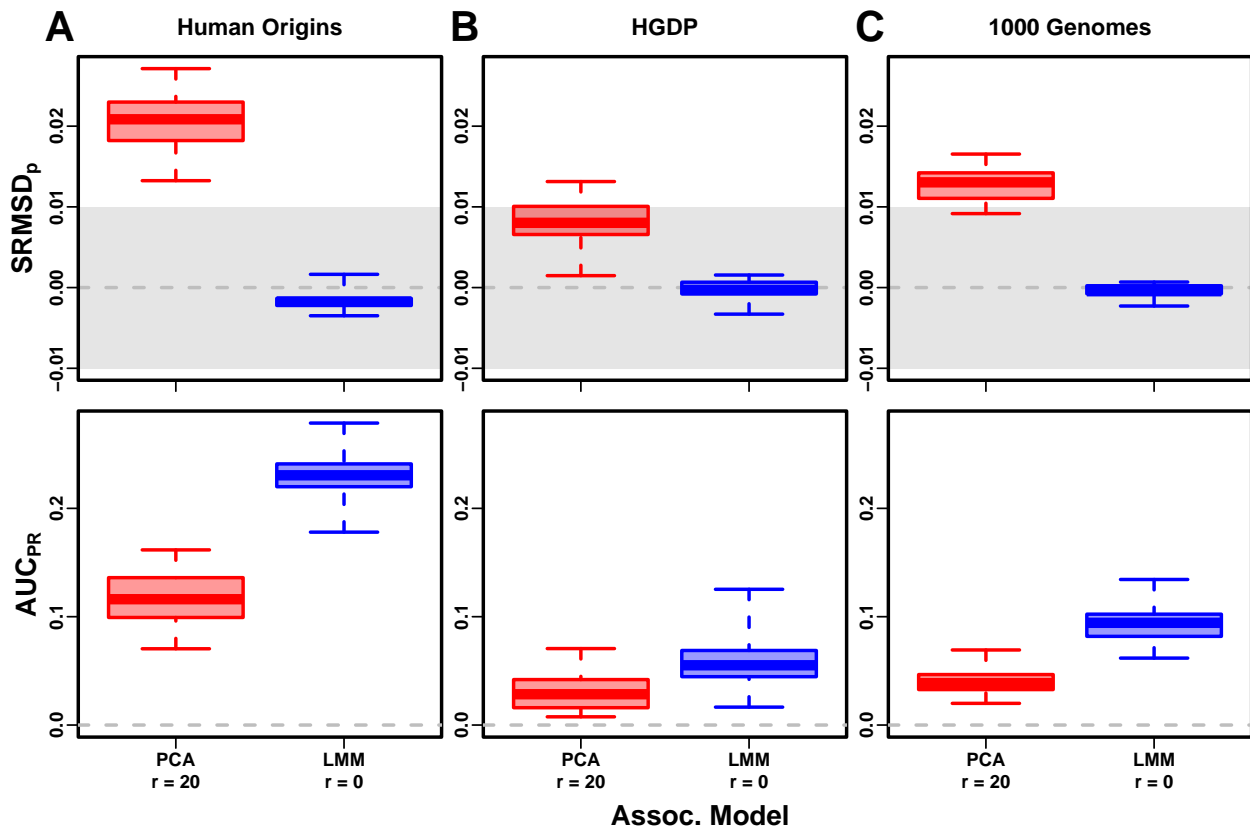


Figure 7: **Evaluation in real datasets excluding 4th degree relatives.** Traits simulated from FES model with high heritability. Each dataset is a column, rows are measures. First row has $|SRMSD_p| < 0.01$ band marked as gray area.

482 3.6 Low heritability and environment simulations

483 Our main evaluations were repeated with traits simulated under a lower heritability value of $h^2 =$
 484 0.3. We reduced the number of causal loci in response to this change in heritability, to result in equal
 485 average effect size per locus compared to the previous high heritability evaluations (see Methods).
 486 Despite that, these low heritability evaluations measured lower AUC_{PR} values than their high
 487 heritability counterparts (Figs. S6 to S10). The gap between LMM and PCA was reduced in these
 488 evaluations, but the main conclusion of the high heritability evaluation holds for low heritability as
 489 well, namely that LMM with $r = 0$ significantly outperforms or ties LMM with $r > 0$ and PCA in
 490 all cases (Table S2).

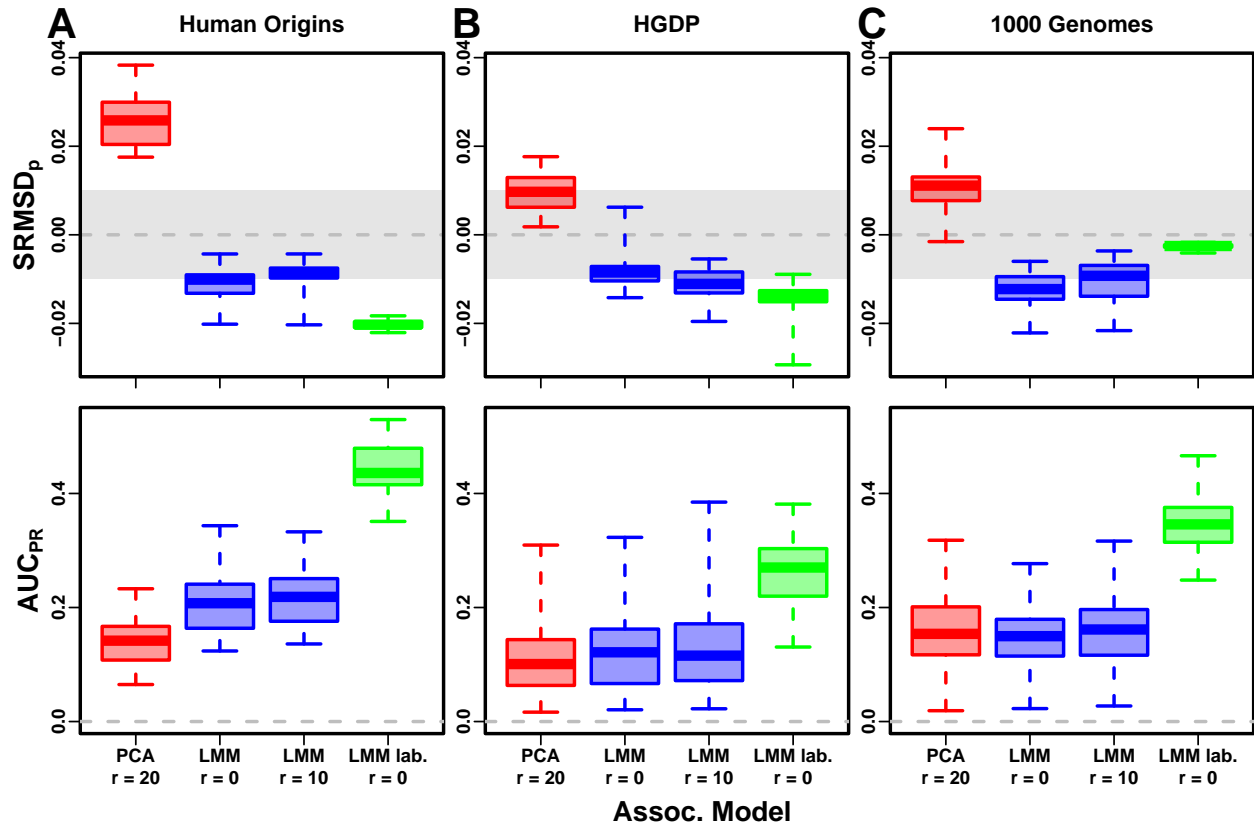


Figure 8: **Evaluation in real datasets excluding 4th degree relatives, FES traits, environment.** Traits simulated with environment effects, otherwise the same as Fig. 7.

491 Lastly, we simulated traits with both low heritability and large environment effects determined

492 by geography and race/ethnicity labels, so they are strongly correlated to the low-dimensional pop-
493 ulation structure (Table 2). For that reason, PCs may be expected to perform better in this setting
494 (in either PCA or LMM). However, we find that both PCA and LMM (even without PCs) increase
495 their AUC_{PR} values compared to the low-heritability evaluations (Fig. S11; Fig. 8 also shows repre-
496 sentative numbers of PCs, which performed optimally or nearly so in individual simulations shown
497 in Figs. S12 to S15). P-value calibration (SRMSD_p) is comparable with or without environment
498 effects, for LMM for all r and for PCA once r is large enough (Fig. S11). These simulations are
499 the only where we occasionally observed for both metrics a significant, though small, advantage
500 of LMM with PCs versus LMM without PCs (Table S3). Additionally, on RC traits only, PCA
501 significantly outperforms LMM in the three real human datasets (Table S3), the only cases in all of
502 our evaluations where this is observed. For comparison, we also evaluate an “oracle” LMM without
503 PCs but with the finest group labels, the same used to simulate environment, as fixed categorical
504 covariates (“LMM lab.”), and see much larger AUC_{PR} values than either LMM with PCs or PCA
505 (Figs. 8 and S12 to S15 and Table S3). However, LMM with labels is often more poorly calibrated
506 than LMM or PCA without labels, which may be since these numerous labels are inappropriately
507 modeled as fixed rather than random effects. Overall, we find that association studies with corre-
508 lated environment and genetic effects remain a challenge for PCA and LMM, that addition of PCs
509 to an LMM improves performance only marginally, and that if the environment effect is driven by
510 geography or ethnicity then use of those labels greatly improves performance compared to using
511 PCs.

512 4 Discussion

513 Our evaluations conclusively determined that LMM without PCs performs better than PCA (for any
514 number of PCs) across all scenarios without environment effects, including all real and simulated
515 genotypes and two trait simulation models. Although the addition of a few PCs to LMM does not
516 greatly hurt its performance (except for small sample sizes), they generally did not improve it either
517 (Tables S2 and 4), which agrees with previous observations [49] but contradicts others [16, 23]. Our
518 findings make sense since PCs are the eigenvectors of the same kinship matrix that parametrizes

519 random effects, so including both is redundant.

520 The presence of environment effects that are correlated to relatedness presents the only sce-
521 nario where occasionally PCA and LMM with PCs outperform LMM without PCs (Table S3). It
522 is commonly believed that PCs model such environment effects well [17–19]. However, we observe
523 that LMM without PCs models environment effects nearly as well as PCs (Fig. 8), consistent with
524 previous findings [32, 33] and with environment inflating heritability estimates using LMM [89].
525 Moreover, modeling the true environment groups as fixed effects always substantially improved
526 AUC_{PR} compared to modeling them with PCs (Fig. 8 and Table S3). Modeling numerous environ-
527 ment groups as fixed effects does result in deflated p-values (Fig. 8 and Table S3), which we expect
528 would be avoided by modeling them as random effects, a strategy we chose not to pursue here as
529 it is both a circular evaluation (the true effects were drawn from that model) and out of scope.
530 Overall, including PCs to model environment effects yields limited power gains if at all, even in an
531 LMM, and is no replacement for more adequate modeling of environment whenever possible.

532 Previous studies found that PCA was better calibrated than LMM for unusually differentiated
533 markers [23, 34, 36], which as simulated were an artificial scenario not based on a population genetics
534 model, and are otherwise believed to be unusual [37, 55]. Our evaluations on real human data,
535 which contain such loci in relevant proportions if they exist, do not replicate that result. Cryptic
536 relatedness strongly favors LMM, an advantage that probably outweighs this potential PCA benefit
537 in real data.

538 Relative to LMM, the behavior of PCA fell between two extremes. When PCA performed well,
539 there was a small number of PCs with both calibrated p-values and AUC_{PR} near that of LMM
540 without PCs. Conversely, PCA performed poorly when no number of PCs had either calibrated
541 p-values or acceptably large AUC_{PR}. There were no cases where high numbers of PCs optimized
542 an acceptable AUC_{PR}, or cases with miscalibrated p-values but high AUC_{PR}. PCA performed well
543 in the admixture simulations (without families, both trait models), real human genotypes with RC
544 traits, and the tree simulations (both trait models). Conversely, PCA performed poorly in the
545 admixed family simulation (both trait models) and the real human genotypes with FES traits.

546 PCA assumes that genetic relatedness is low-dimensional, whereas LMM can handle high-

dimensional relatedness. Thus, PCA performs well in the admixture simulation, which is explicitly low-dimensional (see Materials and Methods), and our tree simulations, which, although complex in principle due to the large number of nodes, had few long branches so a low-dimensional approximation suffices. Conversely, PCA performs poorly under family structure because its kinship matrix is high-dimensional (Fig. S5). However, estimating the dimensionality of real datasets is challenging because estimated eigenvalues have biased distributions. Dimensionality estimated using the Tracy-Widom test [7] did not fully predict the datasets that PCA performs well on. In contrast, estimated local kinship finds considerable cryptic relatedness in all real human datasets and better explains why PCA performs poorly there. The trait model also influences the relative performance of PCA, so genotype-only parameters (eigenvalues or local kinship) alone do not tell the full story.

PCA is at best underpowered relative to LMMs, and at worst miscalibrated regardless of the numbers of PCs included, in real human genotype tests. Among our simulations, such poor performance occurred only in the admixed family. Local kinship estimates reveal considerable family relatedness in the real datasets absent in the corresponding tree simulations. Admixture is also absent in our tree simulations, but our simulations and theory show that admixture is handled well by PCA. Hundreds of close relative pairs have been identified in 1000 Genomes [90–93], but their removal does not improve PCA performance sufficiently in our tests, so the larger number of more distantly related pairs are PCA’s most serious obstacle in practice. Distant relatives are expected to be numerous in any large human dataset [94, 95]. Our FES trait tests show that cryptic relatedness is more challenging when rarer variants have larger coefficients. Overall, the high dimensionality induced by cryptic relatedness is the key challenge for PCA association in modern datasets that is readily overcome by LMM.

Our tests also found PCA robust to large numbers of PCs, far beyond the optimal choice, agreeing with previous anecdotal observations [5, 35], in contrast to using too few PCs for which there is a large performance penalty. The exception was the small sample size simulation, where only small numbers of PCs performed well. In contrast, LMM is simpler since there is no need to choose the number of PCs. However, an LMM with a large number of covariates may have conservative p-values (as observed for LMM with large numbers of PCs), a weakness of the score

575 test used by the LMM we evaluated that may be overcome with other statistical tests. Simulations
576 or post hoc evaluations remain crucial for ensuring that statistics are calibrated.

577 One of the limitations of this work include relatively small sample sizes compared to modern
578 association studies. However, our conclusions are not expected to change with larger sample sizes,
579 as cryptic relatedness will continue to be abundant in such data and thus give LMMs an advantage
580 over PCA. Newer approaches not tested in this work have made LMMs more scalable and applicable
581 to biobank-scale data [38, 46], so one clear next step is carefully evaluating these approaches in
582 simulations with larger sample sizes.

583 The largest limitation of our work is that we only considered quantitative traits. We noted that
584 previous evaluations involving case-control traits tended to report PCA-LMM ties or mixed results,
585 an observation potentially confounded by the use of low-dimensional simulations without family
586 relatedness (Table 1). An additional concern is case-control ascertainment bias, which appears to
587 affect LMMs more severely, although recent work appears to solve this problem [34, 38]. Future
588 evaluations should aim to include our simulations and real datasets, to ensure that previous results
589 were not biased in favor of PCA by employing unrealistic low-dimensional genotype simulations,
590 or by not simulating large coefficients for rare variants expected for diseases by various selection
591 models.

592 Overall, our results lead us to recommend LMM over PCA for association studies in general. Al-
593 though PCA offer flexibility and speed compared to LMM, additional work is required to ensure that
594 PCA is adequate, including removal of close relatives (lowering sample size and wasting resources)
595 followed by simulations or other evaluations of statistics, and even then PCA may perform poorly
596 in terms of both type I error control and power. The large numbers of distant relatives expected of
597 any real dataset all but ensures that PCA will perform poorly compared to LMM. Our findings also
598 suggest that related applications such as polygenic models may enjoy gains in power and accuracy
599 by employing an LMM instead of PCA to model relatedness [21, 87]. PCA remains indispensable
600 across population genetics, from visualizing population structure and performing quality control
601 to its deep connection to admixture models, but the time has come to limit its use in association
602 testing in favor of LMM or other, richer models capable of modeling all forms of relatedness.

603 **5 Appendices**

604 **5.1 Appendix A: Fitting ancestral allele frequency distribution to real data**

605 We calculated \hat{p}_i^T distributions of each real dataset. However, differentiation increases the variance
 606 of these sample \hat{p}_i^T relative to the true p_i^T [31]. We present a new algorithm for constructing an
 607 “undifferentiated” distribution based on the input data but with the lower variance of the true
 608 ancestral distribution. Suppose the p_i^T distribution over loci i satisfies $E[\hat{p}_i^T] = \frac{1}{2}$ and $\text{Var}(p_i^T) =$
 609 V^T . The sample allele frequency \hat{p}_i^T , conditioned on p_i^T , satisfies

$$E[\hat{p}_i^T | p_i^T] = p_i^T, \quad \text{Var}(\hat{p}_i^T | p_i^T) = p_i^T (1 - p_i^T) \bar{\varphi}^T,$$

610 where $\bar{\varphi}^T = \frac{1}{n^2} \sum_{j=1}^n \sum_{k=1}^n \varphi_{jk}^T$ is the mean kinship over all individual [31]. The unconditional
 611 moments of \hat{p}_i^T follow from the laws of total expectation and variance: $E[\hat{p}_i^T] = \frac{1}{2}$ and

$$W^T = \text{Var}(\hat{p}_i^T) = \bar{\varphi}^T \frac{1}{4} + (1 - \bar{\varphi}^T) V^T.$$

612 Since $V^T \leq \frac{1}{4}$ and $\bar{\varphi}^T \geq 0$, then $W^T \geq V^T$. Thus, the goal is to construct a new distribution with
 613 the original, lower variance of

$$614 V^T = \frac{W^T - \frac{1}{4} \bar{\varphi}^T}{1 - \bar{\varphi}^T}. \quad (9)$$

615 We use the unbiased estimator $\hat{W}^T = \frac{1}{m} \sum_{i=1}^m (\hat{p}_i^T - \frac{1}{2})^2$, while $\bar{\varphi}^T$ is calculated from the tree
 616 parameters: the subpopulation coancestry matrix (Eq. (7)), expanded from subpopulations to indi-
 617 viduals, the diagonal converted to kinship (reversing Eq. (8)), and the matrix averaged. However,
 618 since our model ignores the MAF filters imposed in our simulations, $\bar{\varphi}^T$ was adjusted. For Human
 619 Origins the true model $\bar{\varphi}^T$ of 0.143 was used. For 1000 Genomes and HGDP the true $\bar{\varphi}^T$ are 0.126
 620 and 0.124, respectively, but 0.4 for both produced a better fit.

621 Lastly, we construct new allele frequencies,

$$p' = w\hat{p}_i^T + (1 - w)q,$$

622 by a weighted average of \hat{p}_i^T and $q \in (0, 1)$ drawn independently from a different distribution.
623 $E[q] = \frac{1}{2}$ is required to have $E[p'] = \frac{1}{2}$. The resulting variance is

$$\text{Var}(p') = w^2 W^T + (1 - w)^2 \text{Var}(q),$$

624 which we equate to the desired V^T (Eq. (9)) and solve for w . For simplicity, we also set $\text{Var}(q) = V^T$,
625 which is achieved with:

$$q \sim \text{Beta} \left(\frac{1}{2} \left(\frac{1}{4V^T} - 1 \right), \frac{1}{2} \left(\frac{1}{4V^T} - 1 \right) \right).$$

626 Although $w = 0$ yields $\text{Var}(p') = V^T$, we use the second root of the quadratic equation to use \hat{p}_i^T :

$$w = \frac{2V^T}{W^T + V^T}.$$

627 **5.2 Appendix B: comparisons between SRMSD_p, AUC_{PR}, and evaluation mea-
628 sures from the literature**

629 **5.2.1 The inflation factor λ**

630 Test statistic inflation has been used to measure model calibration [1, 23]. The inflation factor
631 λ is defined as the median χ^2 association statistic divided by theoretical median under the null
632 hypothesis [2]. To compare p-values from non- χ^2 tests (such as t-statistics), λ can be calculated
633 from p-values using

$$\lambda = \frac{F^{-1}(1 - p_{\text{median}})}{F^{-1}(1 - u_{\text{median}})},$$

634 where p_{median} is the median observed p-value (including causal loci), $u_{\text{median}} = \frac{1}{2}$ is its null expec-
635 tation, and F is the χ^2 cumulative density function (F^{-1} is the quantile function).

636 To compare λ and SRMSD_p directly, for simplicity assume that all p-values are null. In this
637 case, calibrated p-values give $\lambda = 1$ and SRMSD_p = 0. However, non-uniform p-values with the
638 expected median, such as from genomic control [2], result in $\lambda = 1$, but SRMSD_p ≠ 0 except for
639 uniform p-values, a key flaw of λ that SRMSD_p overcomes. Inflated statistics (anti-conservative

640 p-values) give $\lambda > 1$ and $\text{SRMSD}_p > 0$. Deflated statistics (conservative p-values) give $\lambda < 1$ and
 641 $\text{SRMSD}_p < 0$. Thus, $\lambda \neq 1$ always implies $\text{SRMSD}_p \neq 0$ (where $\lambda - 1$ and SRMSD_p have the
 642 same sign), but not the other way around. Overall, λ depends only on the median p-value, while
 643 SRMSD_p uses the complete distribution. However, SRMSD_p requires knowing which loci are null,
 644 so unlike λ it is only applicable to simulated traits.

645 5.2.2 Empirical comparison of SRMSD_p and λ

646 There is a near one-to-one correspondence between λ and SRMSD_p in our data (Fig. S1). PCA
 647 tended to be inflated ($\lambda > 1$ and $\text{SRMSD}_p > 0$) whereas LMM tended to be deflated ($\lambda < 1$ and
 648 $\text{SRMSD}_p < 0$), otherwise the data for both models fall on the same contiguous curve. We fit a
 649 sigmoidal function to this data,

$$650 \quad \text{SRMSD}_p(\lambda) = a \frac{\lambda^b - 1}{\lambda^b + 1}, \quad (10)$$

651 which for $a, b > 0$ satisfies $\text{SRMSD}_p(\lambda = 1) = 0$ and reflects $\log(\lambda)$ about zero ($\lambda = 1$):

$$\text{SRMSD}_p(\log(\lambda) = -x) = -\text{SRMSD}_p(\log(\lambda) = x).$$

652 We fit this model to $\lambda > 1$ only since it was less noisy and of greater interest, and obtained the
 653 curve shown in Fig. S1 with $a = 0.564$ and $b = 0.619$. The value $\lambda = 1.05$, a common threshold
 654 for benign inflation [23], corresponds to $\text{SRMSD}_p = 0.0085$ according to Eq. (10). Conversely,
 655 $\text{SRMSD}_p = 0.01$, serving as a simpler rule of thumb, corresponds to $\lambda = 1.06$.

656 5.2.3 Type I error rate

657 The type I error rate is the proportion of null p-values with $p \leq t$. Calibrated p-values have type
 658 I error rate near t , which may be evaluated with a binomial test. This measure may give different
 659 results for different t , for example be significantly miscalibrated only for large t (due to lack of power
 660 for smaller t). In contrast, $\text{SRMSD}_p = 0$ guarantees calibrated type I error rates at all t , while large
 661 $|\text{SRMSD}_p|$ indicates incorrect type I errors for a range of t .

662 **5.2.4 Statistical power and comparison to AUC_{PR}**

663 Power is the probability that a test is declared significant when the alternative hypothesis H_1 holds.

664 At a p-value threshold t , power equals

$$F(t) = \Pr(p < t | H_1).$$

665 $F(t)$ is a cumulative function, so it is monotonically increasing and has an inverse. Like type I error

666 control, power may rank models differently depending on t .

667 Power is not meaningful when p-values are not calibrated. To establish a clear connection to

668 AUC_{PR}, assume calibrated (uniform) null p-values: $\Pr(p < t | H_0) = t$. TPs, FPs, and FNs at t are

$$\text{TP}(t) = m\pi_1 F(t),$$

$$\text{FP}(t) = m\pi_0 t,$$

$$\text{FN}(t) = m\pi_1(1 - F(t)),$$

669 where $\pi_0 = \Pr(H_0)$ is the proportion of null cases and $\pi_1 = 1 - \pi_0$ of alternative cases. Therefore,

$$\text{Precision}(t) = \frac{\pi_1 F(t)}{\pi_1 F(t) + \pi_0 t},$$

$$\text{Recall}(t) = F(t).$$

670 Noting that $t = F^{-1}(\text{Recall})$, precision can be written as a function of recall, the power function,

671 and constants:

$$\text{Precision}(\text{Recall}) = \frac{\pi_1 \text{Recall}}{\pi_1 \text{Recall} + \pi_0 F^{-1}(\text{Recall})}.$$

672 This last form leads most clearly to $\text{AUC}_{\text{PR}} = \int_0^1 \text{Precision}(\text{Recall}) d\text{Recall}$.

673 Lastly, consider a simple yet common case in which model A is uniformly more powerful than

674 model B : $F_A(t) > F_B(t)$ for every t . Therefore $F_A^{-1}(\text{Recall}) < F_B^{-1}(\text{Recall})$ for every recall value.

675 This ensures that the precision of A is greater than that of B at every recall value, so AUC_{PR} is

676 greater for A than B . Thus, AUC_{PR} ranks calibrated models according to power.

677 Competing interests

678 The authors declare no competing interests.

679 Acknowledgments

680 This work was funded in part by the Duke University School of Medicine Whitehead Scholars
681 Program, a gift from the Whitehead Charitable Foundation. The 1000 Genomes data were generated
682 at the New York Genome Center with funds provided by NHGRI Grant 3UM1HG008901-03S1.

683 Web resources

684 plink2, <https://www.cog-genomics.org/plink/2.0/>

685 GCTA, <https://yanglab.westlake.edu.cn/software/gcta/>

686 Eigensoft, <https://github.com/DReichLab/EIG>

687 bnpsd, <https://cran.r-project.org/package=bnpsd>

688 simfam, <https://cran.r-project.org/package=simfam>

689 simtrait, <https://cran.r-project.org/package=simtrait>

690 genio, <https://cran.r-project.org/package=genio>

691 popkin, <https://cran.r-project.org/package=popkin>

692 ape, <https://cran.r-project.org/package=ape>

693 nnls, <https://cran.r-project.org/package=nnls>

694 PRROC, <https://cran.r-project.org/package=PRROC>

695 BEDMatrix, <https://cran.r-project.org/package=BEDMatrix>

696 **Data and code availability**

697 The data and code generated during this study are available on GitHub at <https://github.com/>
698 OchoaLab/pca-assoc-paper. The public subset of Human Origins is available on the Reich Lab
699 website at <https://reich.hms.harvard.edu/datasets>; non-public samples have to be requested
700 from David Reich. The WGS version of HGDP was downloaded from the Wellcome Sanger In-
701 stitute FTP site at ftp://ngs.sanger.ac.uk/production/hgdp/hgdp_wgs.20190516/. The high-
702 coverage version of the 1000 Genomes Project was downloaded from [ftp://ftp.1000genomes.ebi.
703 ac.uk/vol1/ftp/data_collections/1000G_2504_high_coverage/working/20190425_NYGC_GATK/](ftp://ftp.1000genomes.ebi.ac.uk/vol1/ftp/data_collections/1000G_2504_high_coverage/working/20190425_NYGC_GATK/).

704 **References**

- 705 [1] W. Astle and D. J. Balding. “Population Structure and Cryptic Relatedness in Genetic Asso-
706 ciation Studies”. *Statist. Sci.* 24(4) (2009), pp. 451–471. DOI: [10.1214/09-STS307](https://doi.org/10.1214/09-STS307).
- 707 [2] B. Devlin and K. Roeder. “Genomic Control for Association Studies”. *Biometrics* 55(4) (1999),
708 pp. 997–1004. DOI: [10.1111/j.0006-341X.1999.00997.x](https://doi.org/10.1111/j.0006-341X.1999.00997.x).
- 709 [3] B. F. Voight and J. K. Pritchard. “Confounding from Cryptic Relatedness in Case-Control
710 Association Studies”. *PLOS Genetics* 1(3) (2005), e32. DOI: [10.1371/journal.pgen.0010032](https://doi.org/10.1371/journal.pgen.0010032).
- 711 [4] S. Zhang, X. Zhu, and H. Zhao. “On a semiparametric test to detect associations between
712 quantitative traits and candidate genes using unrelated individuals”. *Genetic Epidemiology*
713 24(1) (2003), pp. 44–56. DOI: [10.1002/gepi.10196](https://doi.org/10.1002/gepi.10196).
- 714 [5] A. L. Price et al. “Principal components analysis corrects for stratification in genome-wide
715 association studies”. *Nat. Genet.* 38(8) (2006), pp. 904–909. DOI: [10.1038/ng1847](https://doi.org/10.1038/ng1847).
- 716 [6] M. Bouaziz, C. Ambroise, and M. Guedj. “Accounting for Population Stratification in Practice:
717 A Comparison of the Main Strategies Dedicated to Genome-Wide Association Studies”. *PLOS
718 ONE* 6(12) (2011), e28845. DOI: [10.1371/journal.pone.0028845](https://doi.org/10.1371/journal.pone.0028845).
- 719 [7] N. Patterson, A. L. Price, and D. Reich. “Population Structure and Eigenanalysis”. *PLoS
720 Genet* 2(12) (2006), e190. DOI: [10.1371/journal.pgen.0020190](https://doi.org/10.1371/journal.pgen.0020190).

- 721 [8] I. T. Jolliffe. *Principal Component Analysis*. 2nd ed. New York: Springer-Verlag, 2002.
- 722 [9] J. K. Pritchard et al. “Association Mapping in Structured Populations”. *The American Journal*
723 *of Human Genetics* 67(1) (2000), pp. 170–181. DOI: 10.1086/302959.
- 724 [10] D. H. Alexander, J. Novembre, and K. Lange. “Fast model-based estimation of ancestry in
725 unrelated individuals”. *Genome Res.* 19(9) (2009), pp. 1655–1664. DOI: 10.1101/gr.094052.
726 109.
- 727 [11] Q. Zhou, L. Zhao, and Y. Guan. “Strong Selection at MHC in Mexicans since Admixture”.
728 *PLoS Genet.* 12(2) (2016), e1005847. DOI: 10.1371/journal.pgen.1005847.
- 729 [12] G. McVean. “A genealogical interpretation of principal components analysis”. *PLoS Genet*
730 5(10) (2009), e1000686. DOI: 10.1371/journal.pgen.1000686.
- 731 [13] X. Zheng and B. S. Weir. “Eigenanalysis of SNP data with an identity by descent interpreta-
732 tion”. *Theor Popul Biol* 107 (2016), pp. 65–76. DOI: 10.1016/j.tpb.2015.09.004.
- 733 [14] I. Cabreros and J. D. Storey. “A Likelihood-Free Estimator of Population Structure Bridging
734 Admixture Models and Principal Components Analysis”. *Genetics* 212(4) (2019), pp. 1009–
735 1029. DOI: 10.1534/genetics.119.302159.
- 736 [15] A. M. Chiu et al. “Inferring population structure in biobank-scale genomic data”. *The Amer-*
737 *ican Journal of Human Genetics* 0(0) (2022). DOI: 10.1016/j.ajhg.2022.02.015.
- 738 [16] K. Zhao et al. “An Arabidopsis Example of Association Mapping in Structured Samples”.
739 *PLOS Genetics* 3(1) (2007), e4. DOI: 10.1371/journal.pgen.0030004.
- 740 [17] J. Novembre et al. “Genes mirror geography within Europe”. *Nature* 456(7218) (2008), pp. 98–
741 101. DOI: 10.1038/nature07331.
- 742 [18] Y. Zhang and W. Pan. “Principal Component Regression and Linear Mixed Model in Associ-
743 ation Analysis of Structured Samples: Competitors or Complements?” *Genetic Epidemiology*
744 39(3) (2015), pp. 149–155. DOI: 10.1002/gepi.21879.
- 745 [19] M. Lin et al. “Admixed Populations Improve Power for Variant Discovery and Portability in
746 Genome-Wide Association Studies”. *Frontiers in Genetics* 12 (2021).

- 747 [20] H. Xu and Y. Guan. “Detecting Local Haplotype Sharing and Haplotype Association”. *Ge-*
748 *netics* 197(3) (2014), pp. 823–838. DOI: 10.1534/genetics.114.164814.
- 749 [21] J. Qian et al. “A fast and scalable framework for large-scale and ultrahigh-dimensional sparse
750 regression with application to the UK Biobank”. *PLOS Genetics* 16(10) (2020), e1009141.
751 DOI: 10.1371/journal.pgen.1009141.
- 752 [22] T. Thornton and M. S. McPeek. “ROADTRIPS: case-control association testing with partially
753 or completely unknown population and pedigree structure”. *Am. J. Hum. Genet.* 86(2) (2010),
754 pp. 172–184. DOI: 10.1016/j.ajhg.2010.01.001.
- 755 [23] A. L. Price et al. “New approaches to population stratification in genome-wide association
756 studies”. *Nature Reviews Genetics* 11(7) (2010), pp. 459–463. DOI: 10.1038/nrg2813.
- 757 [24] S. Lee et al. “Sparse Principal Component Analysis for Identifying Ancestry-Informative Mark-
758 ers in Genome-Wide Association Studies”. *Genetic Epidemiology* 36(4) (2012), pp. 293–302.
759 DOI: 10.1002/gepi.21621.
- 760 [25] G. Abraham and M. Inouye. “Fast Principal Component Analysis of Large-Scale Genome-
761 Wide Data”. *PLOS ONE* 9(4) (2014), e93766. DOI: 10.1371/journal.pone.0093766.
- 762 [26] K. Galinsky et al. “Fast Principal-Component Analysis Reveals Convergent Evolution of
763 ADH1B in Europe and East Asia”. *The American Journal of Human Genetics* 98(3) (2016),
764 pp. 456–472. DOI: 10.1016/j.ajhg.2015.12.022.
- 765 [27] G. Abraham, Y. Qiu, and M. Inouye. “FlashPCA2: principal component analysis of Biobank-
766 scale genotype datasets”. *Bioinformatics* 33(17) (2017), pp. 2776–2778. DOI: 10.1093/bioinformatics/
767 btx299.
- 768 [28] A. Agrawal et al. “Scalable probabilistic PCA for large-scale genetic variation data”. *PLOS*
769 *Genetics* 16(5) (2020), e1008773. DOI: 10.1371/journal.pgen.1008773.
- 770 [29] J. Yu et al. “A unified mixed-model method for association mapping that accounts for multiple
771 levels of relatedness”. *Nat. Genet.* 38(2) (2006), pp. 203–208. DOI: 10.1038/ng1702.
- 772 [30] H. M. Kang et al. “Efficient control of population structure in model organism association
773 mapping”. *Genetics* 178(3) (2008), pp. 1709–1723. DOI: 10.1534/genetics.107.080101.

- 774 [31] A. Ochoa and J. D. Storey. “Estimating FST and kinship for arbitrary population structures”.
775 *PLoS Genet* 17(1) (2021), e1009241. DOI: 10.1371/journal.pgen.1009241.
- 776 [32] B. J. Vilhjálmsson and M. Nordborg. “The nature of confounding in genome-wide association
777 studies”. *Nat Rev Genet* 14(1) (2013), pp. 1–2. DOI: 10.1038/nrg3382.
- 778 [33] H. Wang, B. Aragam, and E. P. Xing. “Trade-offs of Linear Mixed Models in Genome-Wide
779 Association Studies”. *Journal of Computational Biology* 29(3) (2022), pp. 233–242. DOI: 10.
780 1089/cmb.2021.0157.
- 781 [34] J. Yang et al. “Advantages and pitfalls in the application of mixed-model association methods”.
782 *Nat Genet* 46(2) (2014), pp. 100–106. DOI: 10.1038/ng.2876.
- 783 [35] H. M. Kang et al. “Variance component model to account for sample structure in genome-wide
784 association studies”. *Nat. Genet.* 42(4) (2010), pp. 348–354. DOI: 10.1038/ng.548.
- 785 [36] C. Wu et al. “A Comparison of Association Methods Correcting for Population Stratification
786 in Case–Control Studies”. *Annals of Human Genetics* 75(3) (2011), pp. 418–427. DOI: 10.
787 1111/j.1469-1809.2010.00639.x.
- 788 [37] J. H. Sul and E. Eskin. “Mixed models can correct for population structure for genomic regions
789 under selection”. *Nature Reviews Genetics* 14(4) (2013), p. 300. DOI: 10.1038/nrg2813-c1.
- 790 [38] W. Zhou et al. “Efficiently controlling for case-control imbalance and sample relatedness in
791 large-scale genetic association studies”. *Nat Genet* 50(9) (2018), pp. 1335–1341. DOI: 10.1038/
792 s41588-018-0184-y.
- 793 [39] Y. S. Aulchenko, D.-J. de Koning, and C. Haley. “Genomewide rapid association using mixed
794 model and regression: a fast and simple method for genomewide pedigree-based quantitative
795 trait loci association analysis”. *Genetics* 177(1) (2007), pp. 577–585. DOI: 10.1534/genetics.
796 107.075614.
- 797 [40] Z. Zhang et al. “Mixed linear model approach adapted for genome-wide association studies”.
798 *Nat Genet* 42(4) (2010), pp. 355–360. DOI: 10.1038/ng.546.
- 799 [41] C. Lippert et al. “FaST linear mixed models for genome-wide association studies”. *Nat. Meth-*
800 *ods* 8(10) (2011), pp. 833–835. DOI: 10.1038/nmeth.1681.

- 801 [42] J. Yang et al. “GCTA: a tool for genome-wide complex trait analysis”. *Am. J. Hum. Genet.*
802 88(1) (2011), pp. 76–82. DOI: 10.1016/j.ajhg.2010.11.011.
- 803 [43] J. Listgarten et al. “Improved linear mixed models for genome-wide association studies”. *Nat*
804 *Methods* 9(6) (2012), pp. 525–526. DOI: 10.1038/nmeth.2037.
- 805 [44] X. Zhou and M. Stephens. “Genome-wide efficient mixed-model analysis for association stud-
806 ies”. *Nat. Genet.* 44(7) (2012), pp. 821–824. DOI: 10.1038/ng.2310.
- 807 [45] G. R. Svishcheva et al. “Rapid variance components-based method for whole-genome associ-
808 ation analysis”. *Nat Genet* 44(10) (2012), pp. 1166–1170. DOI: 10.1038/ng.2410.
- 809 [46] P.-R. Loh et al. “Efficient Bayesian mixed-model analysis increases association power in large
810 cohorts”. *Nat. Genet.* 47(3) (2015), pp. 284–290. DOI: 10.1038/ng.3190.
- 811 [47] G. E. Hoffman. “Correcting for population structure and kinship using the linear mixed model:
812 theory and extensions”. *PLoS ONE* 8(10) (2013), e75707. DOI: 10.1371/journal.pone.
813 0075707.
- 814 [48] G. Tucker, A. L. Price, and B. Berger. “Improving the Power of GWAS and Avoiding Con-
815 founding from Population Stratification with PC-Select”. *Genetics* 197(3) (2014), pp. 1045–
816 1049. DOI: 10.1534/genetics.114.164285.
- 817 [49] N. Liu et al. “Controlling Population Structure in Human Genetic Association Studies with
818 Samples of Unrelated Individuals”. *Stat Interface* 4(3) (2011), pp. 317–326. DOI: 10.4310/
819 sii.2011.v4.n3.a6.
- 820 [50] J. Zeng et al. “Signatures of negative selection in the genetic architecture of human complex
821 traits”. *Nature Genetics* 50(5) (2018), pp. 746–753. DOI: 10.1038/s41588-018-0101-4.
- 822 [51] J. Mbatchou et al. “Computationally efficient whole-genome regression for quantitative and
823 binary traits”. *Nat Genet* 53(7) (2021), pp. 1097–1103. DOI: 10.1038/s41588-021-00870-7.
- 824 [52] M. Song, W. Hao, and J. D. Storey. “Testing for genetic associations in arbitrarily structured
825 populations”. *Nat. Genet.* 47(5) (2015), pp. 550–554. DOI: 10.1038/ng.3244.

- 826 [53] X. Liu et al. “Iterative Usage of Fixed and Random Effect Models for Powerful and Efficient
827 Genome-Wide Association Studies”. *PLOS Genet* 12(2) (2016), e1005767. DOI: 10.1371/journal.pgen.1005767.
- 828
- 829 [54] J. H. Sul, L. S. Martin, and E. Eskin. “Population structure in genetic studies: Confounding
830 factors and mixed models”. *PLoS Genet.* 14(12) (2018), e1007309. DOI: 10.1371/journal.pgen.1007309.
- 831
- 832 [55] A. L. Price et al. “Response to Sul and Eskin”. *Nature Reviews Genetics* 14(4) (2013), p. 300.
833 DOI: 10.1038/nrg2813-c2.
- 834 [56] T. G. P. Consortium. “A map of human genome variation from population-scale sequencing”.
835 *Nature* 467(7319) (2010), pp. 1061–1073. DOI: 10.1038/nature09534.
- 836 [57] 1000 Genomes Project Consortium et al. “An integrated map of genetic variation from 1,092
837 human genomes”. *Nature* 491(7422) (2012), pp. 56–65. DOI: 10.1038/nature11632.
- 838 [58] H. M. Cann et al. “A human genome diversity cell line panel”. *Science* 296(5566) (2002),
839 pp. 261–262. DOI: 10.1126/science.296.5566.261b.
- 840 [59] N. A. Rosenberg et al. “Genetic Structure of Human Populations”. *Science* 298(5602) (2002),
841 pp. 2381–2385. DOI: 10.1126/science.1078311.
- 842 [60] A. Bergström et al. “Insights into human genetic variation and population history from 929
843 diverse genomes”. *Science* 367(6484) (2020). DOI: 10.1126/science.aay5012.
- 844 [61] N. Patterson et al. “Ancient admixture in human history”. *Genetics* 192(3) (2012), pp. 1065–
845 1093. DOI: 10.1534/genetics.112.145037.
- 846 [62] I. Lazaridis et al. “Ancient human genomes suggest three ancestral populations for present-day
847 Europeans”. *Nature* 513(7518) (2014), pp. 409–413. DOI: 10.1038/nature13673.
- 848 [63] I. Lazaridis et al. “Genomic insights into the origin of farming in the ancient Near East”.
849 *Nature* 536(7617) (2016), pp. 419–424. DOI: 10.1038/nature19310.
- 850 [64] P. Skoglund et al. “Genomic insights into the peopling of the Southwest Pacific”. *Nature*
851 538(7626) (2016), pp. 510–513. DOI: 10.1038/nature19844.

- 852 [65] J.-H. Park et al. “Distribution of allele frequencies and effect sizes and their interrelationships
853 for common genetic susceptibility variants”. *PNAS* 108(44) (2011), pp. 18026–18031. DOI:
854 10.1073/pnas.1114759108.
- 855 [66] L. J. O’Connor et al. “Extreme Polygenicity of Complex Traits Is Explained by Negative
856 Selection”. *The American Journal of Human Genetics* 0(0) (2019). DOI: 10.1016/j.ajhg.
857 2019.07.003.
- 858 [67] Y. B. Simons et al. “A population genetic interpretation of GWAS findings for human quanti-
859 tative traits”. *PLOS Biology* 16(3) (2018), e2002985. DOI: 10.1371/journal.pbio.2002985.
- 860 [68] G. Malécot. *Mathématiques de l'hérédité*. Masson et Cie, 1948.
- 861 [69] S. Wright. “The Genetical Structure of Populations”. *Annals of Eugenics* 15(1) (1949), pp. 323–
862 354. DOI: 10.1111/j.1469-1809.1949.tb02451.x.
- 863 [70] A. Jacquard. *Structures génétiques des populations*. Paris: Masson et Cie, 1970.
- 864 [71] A. Ochoa and J. D. Storey. *New kinship and FST estimates reveal higher levels of differenti-
865 ation in the global human population*. 2019. DOI: 10.1101/653279.
- 866 [72] Z. Hou and A. Ochoa. *Genetic association models are robust to common population kinship
867 estimation biases*. 2022. DOI: 10.1101/2022.11.07.515490.
- 868 [73] C. C. Chang et al. “Second-generation PLINK: rising to the challenge of larger and richer
869 datasets”. *GigaScience* 4(1) (2015), p. 7. DOI: 10.1186/s13742-015-0047-8.
- 870 [74] D. J. Balding and R. A. Nichols. “A method for quantifying differentiation between populations
871 at multi-allelic loci and its implications for investigating identity and paternity”. *Genetica*
872 96(1-2) (1995), pp. 3–12. DOI: <https://doi.org/10.1007/BF01441146>.
- 873 [75] E. Paradis and K. Schliep. “ape 5.0: an environment for modern phylogenetics and evolutionary
874 analyses in R”. *Bioinformatics* 35(3) (2019), pp. 526–528. DOI: 10.1093/bioinformatics/
875 bty633.
- 876 [76] R. R. Sokal and C. D. Michener. “A statistical method for evaluating systematic relationships.”
877 *Univ. Kansas, Sci. Bull.* 38 (1958), pp. 1409–1438.

- 878 [77] C. L. Lawson and R. J. Hanson. *Solving least squares problems*. Englewood Cliffs: Prentice
879 Hall, 1974.
- 880 [78] K. M. Mullen and I. H. M. v. Stokkum. *npls: The Lawson-Hanson algorithm for non-negative
881 least squares (NPLS)*. 2012.
- 882 [79] J.-H. Park et al. “Estimation of effect size distribution from genome-wide association studies
883 and implications for future discoveries”. *Nature Genetics* 42(7) (2010), pp. 570–575. DOI:
884 10.1038/ng.610.
- 885 [80] A. Grueneberg and G. d. l. Campos. “BGData - A Suite of R Packages for Genomic Analysis
886 with Big Data”. *G3: Genes, Genomes, Genetics* 9(5) (2019), pp. 1377–1383. DOI: 10.1534/
887 g3.119.400018.
- 888 [81] S. Fairley et al. “The International Genome Sample Resource (IGSR) collection of open human
889 genomic variation resources”. *Nucleic Acids Research* 48(D1) (2020), pp. D941–D947. DOI:
890 10.1093/nar/gkz836.
- 891 [82] A. Manichaikul et al. “Robust relationship inference in genome-wide association studies”.
892 *Bioinformatics* 26(22) (2010), pp. 2867–2873. DOI: 10.1093/bioinformatics/btq559.
- 893 [83] J. D. Storey. “The positive false discovery rate: a Bayesian interpretation and the q-value”.
894 *Ann. Statist.* 31(6) (2003), pp. 2013–2035. DOI: 10.1214/aos/1074290335.
- 895 [84] J. D. Storey and R. Tibshirani. “Statistical significance for genomewide studies”. *Proceedings
896 of the National Academy of Sciences of the United States of America* 100(16) (2003), pp. 9440–
897 9445. DOI: 10.1073/pnas.1530509100.
- 898 [85] J. Grau, I. Grosse, and J. Keilwagen. “PRROC: computing and visualizing precision-recall and
899 receiver operating characteristic curves in R”. *Bioinformatics* 31(15) (2015), pp. 2595–2597.
900 DOI: 10.1093/bioinformatics/btv153.
- 901 [86] P. Gopalan et al. “Scaling probabilistic models of genetic variation to millions of humans”.
902 *Nat. Genet.* 48(12) (2016), pp. 1587–1590. DOI: 10.1038/ng.3710.

- 903 [87] B. Rakitsch et al. “A Lasso multi-marker mixed model for association mapping with population
904 structure correction”. *Bioinformatics* 29(2) (2013), pp. 206–214. DOI: 10.1093/bioinformatics/
905 bts669.
- 906 [88] M. Conomos et al. “Model-free Estimation of Recent Genetic Relatedness”. *The American
907 Journal of Human Genetics* 98(1) (2016), pp. 127–148. DOI: 10.1016/j.ajhg.2015.11.022.
- 908 [89] D. Heckerman et al. “Linear mixed model for heritability estimation that explicitly addresses
909 environmental variation”. *Proc. Natl. Acad. Sci. U.S.A.* 113(27) (2016), pp. 7377–7382. DOI:
910 10.1073/pnas.1510497113.
- 911 [90] S. Gazal et al. “High level of inbreeding in final phase of 1000 Genomes Project”. *Sci Rep* 5(1)
912 (2015), p. 17453. DOI: 10.1038/srep17453.
- 913 [91] A. Al-Khudhair et al. “Inference of Distant Genetic Relations in Humans Using “1000 Genomes””.
914 *Genome Biology and Evolution* 7(2) (2015), pp. 481–492. DOI: 10.1093/gbe/evv003.
- 915 [92] L. Fedorova et al. “Atlas of Cryptic Genetic Relatedness Among 1000 Human Genomes”.
916 *Genome Biology and Evolution* 8(3) (2016), pp. 777–790. DOI: 10.1093/gbe/evw034.
- 917 [93] D. Schlauch, H. Fier, and C. Lange. “Identification of genetic outliers due to sub-structure
918 and cryptic relationships”. *Bioinformatics* 33(13) (2017), pp. 1972–1979. DOI: 10.1093/
919 bioinformatics/btx109.
- 920 [94] B. M. Henn et al. “Cryptic Distant Relatives Are Common in Both Isolated and Cosmopolitan
921 Genetic Samples”. *PLOS ONE* 7(4) (2012), e34267. DOI: 10.1371/journal.pone.0034267.
- 922 [95] V. Shchur and R. Nielsen. “On the number of siblings and p-th cousins in a large population
923 sample”. *J Math Biol* 77(5) (2018), pp. 1279–1298. DOI: 10.1007/s00285-018-1252-8.

Supplemental figures

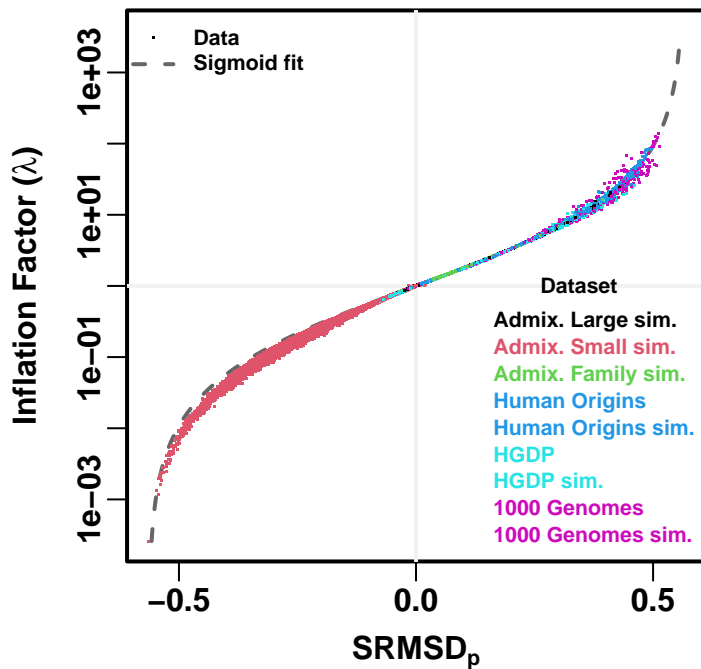


Figure S1: **Comparison between SRMSD_p and inflation factor.** Each point is a pair of statistics for one replicate, one association model (PCA or LMM with some number of PCs r), one trait model (FES vs RC, all heritability/environments tested), and one dataset (color coded by dataset). Note log y-axis (λ). The sigmoidal curve in Eq. (10) is fit to the data.

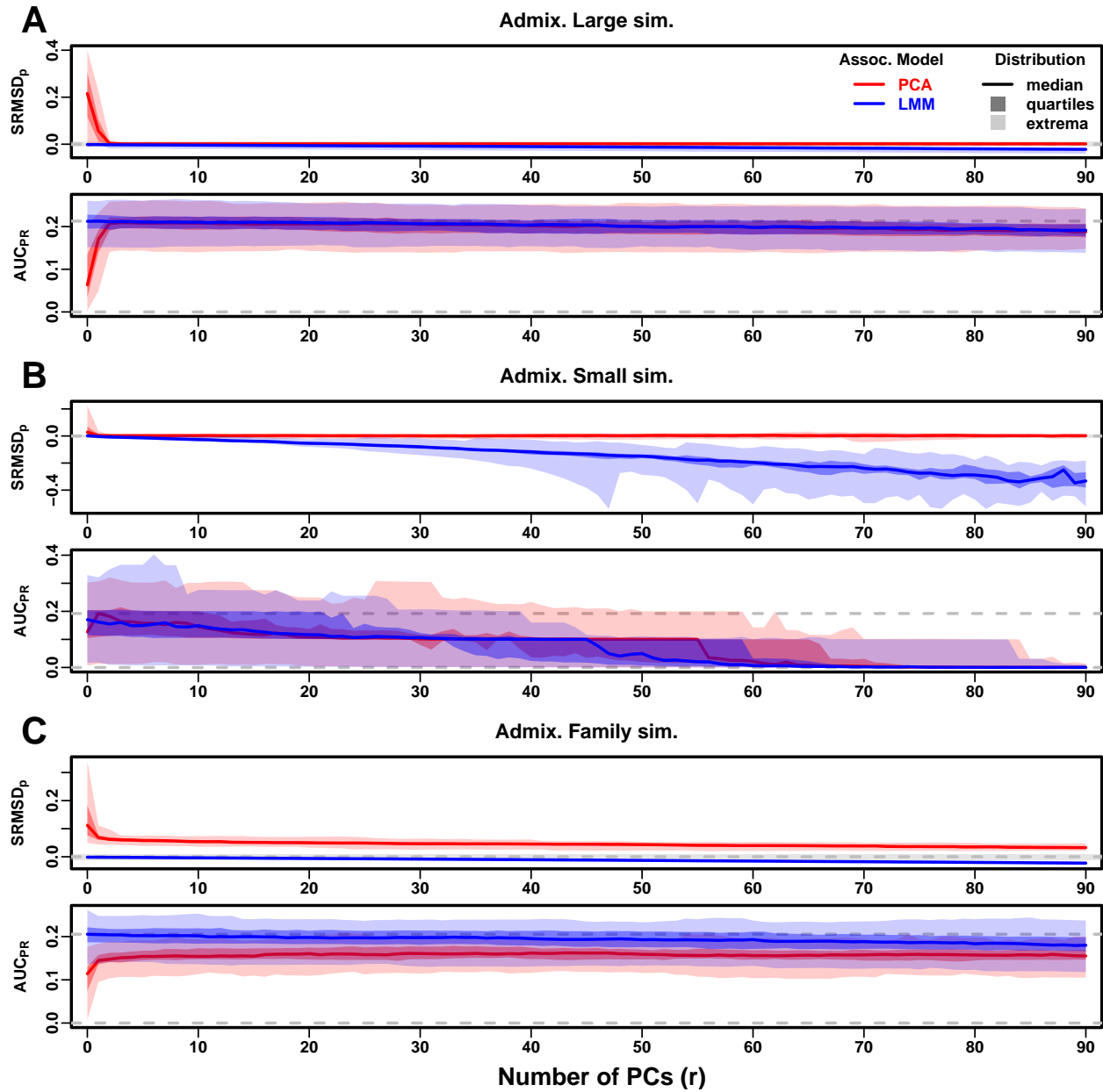


Figure S2: **Evaluations in admixture simulations with RC traits.** Traits simulated from RC model, otherwise the same as Fig. 3.

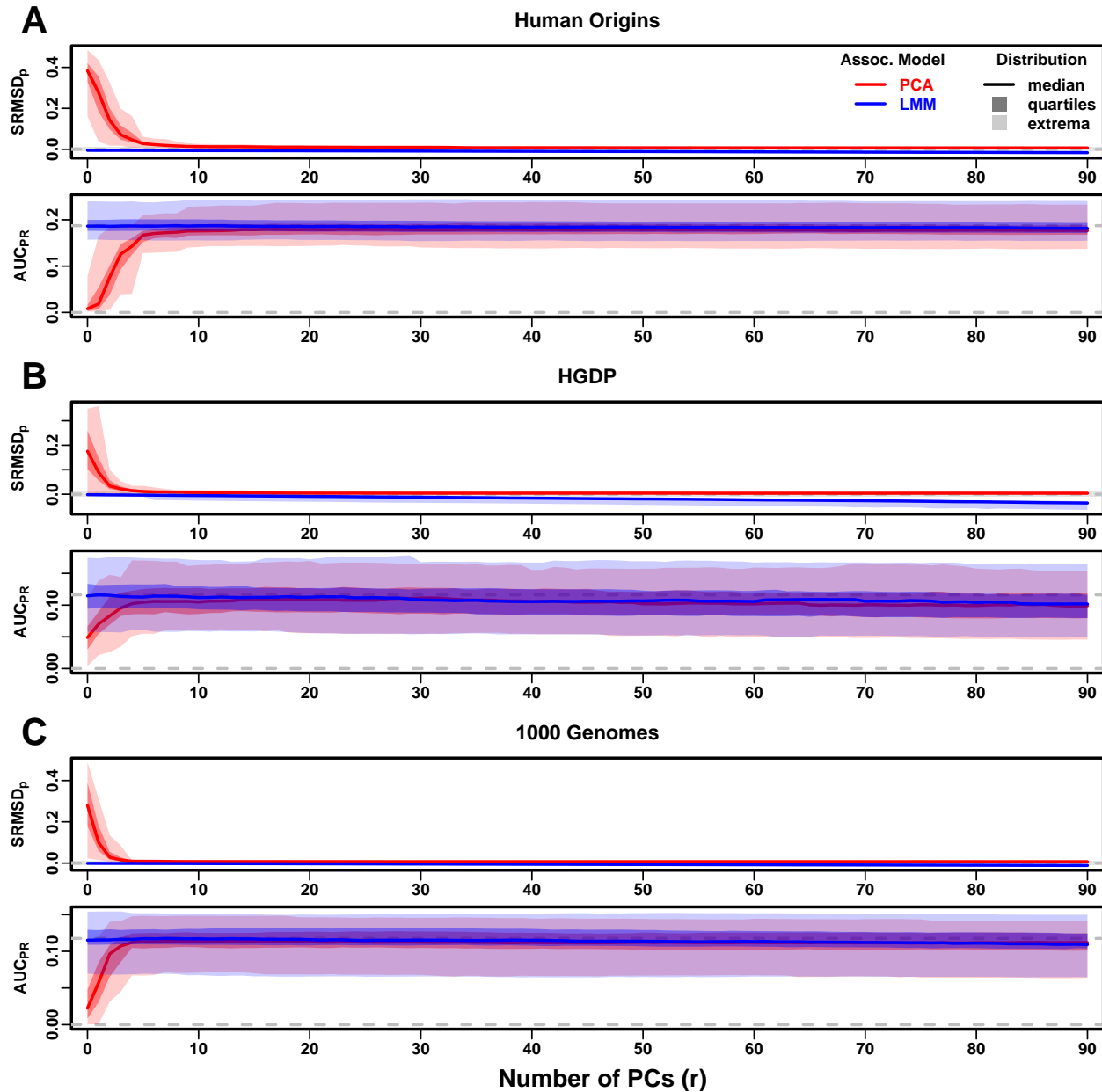


Figure S3: Evaluations in real human genotype datasets with RC traits. Traits simulated from RC model, otherwise the same as Fig. 4.

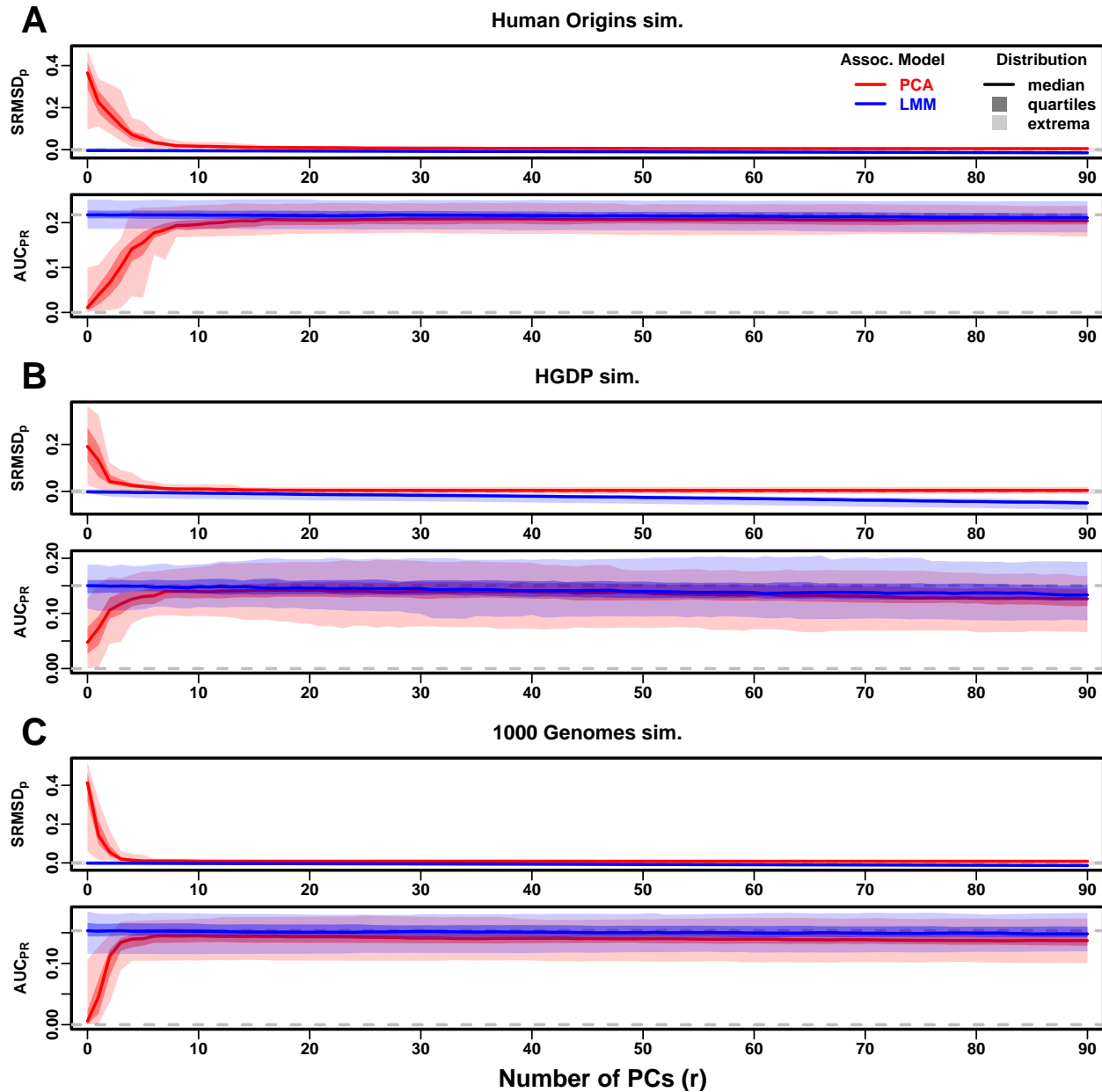


Figure S4: Evaluations in tree simulations fit to human data with RC traits. Traits simulated from RC model, otherwise the same as Fig. 5.

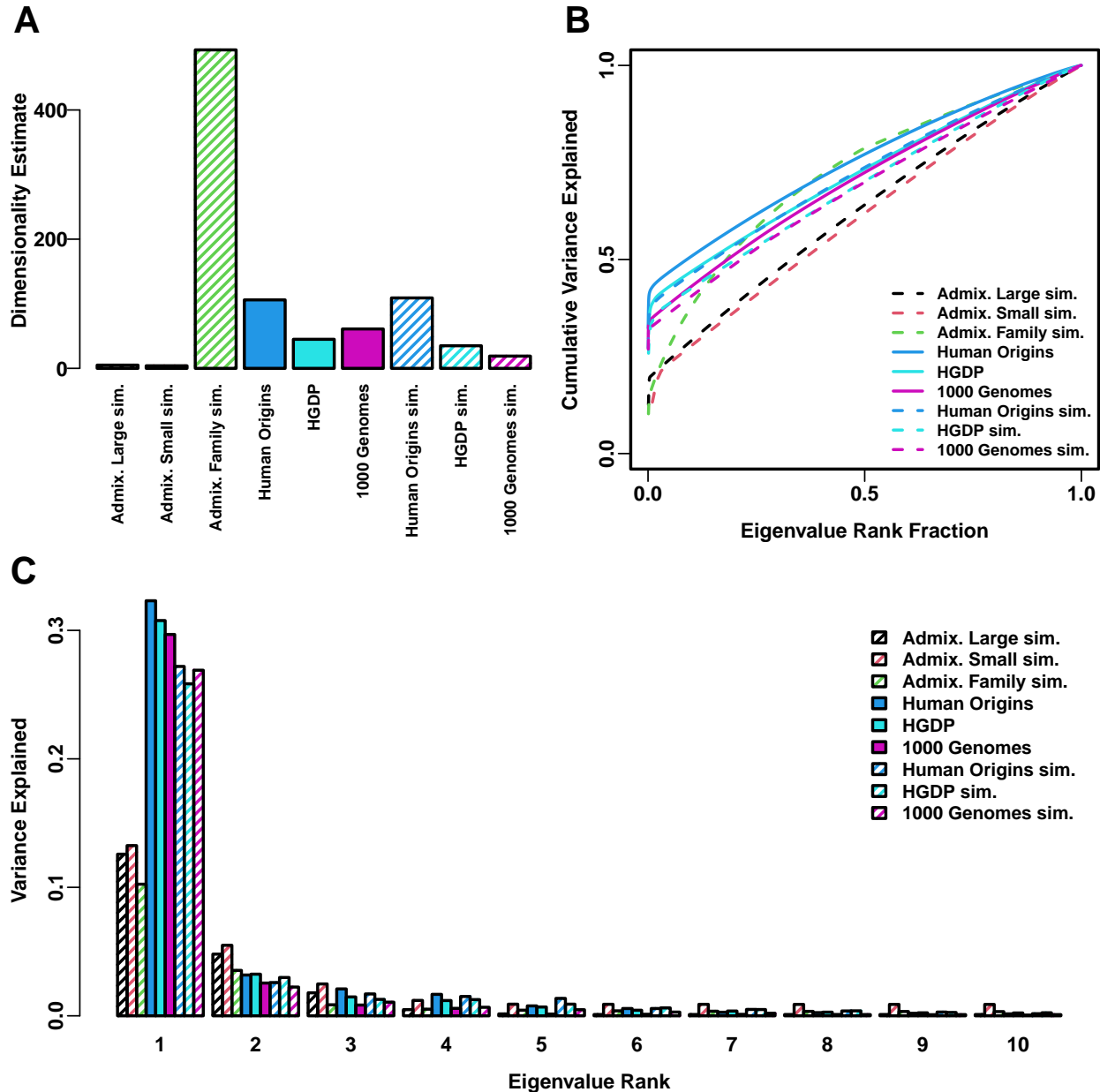


Figure S5: **Estimated dimensionality of datasets.** **A.** Kinship dimensionalities estimated with the Tracy-Widom test with $p < 0.01$. **B.** Cumulative variance explained versus eigenvalue rank fraction. **C.** Variance explained by first 10 eigenvalues.

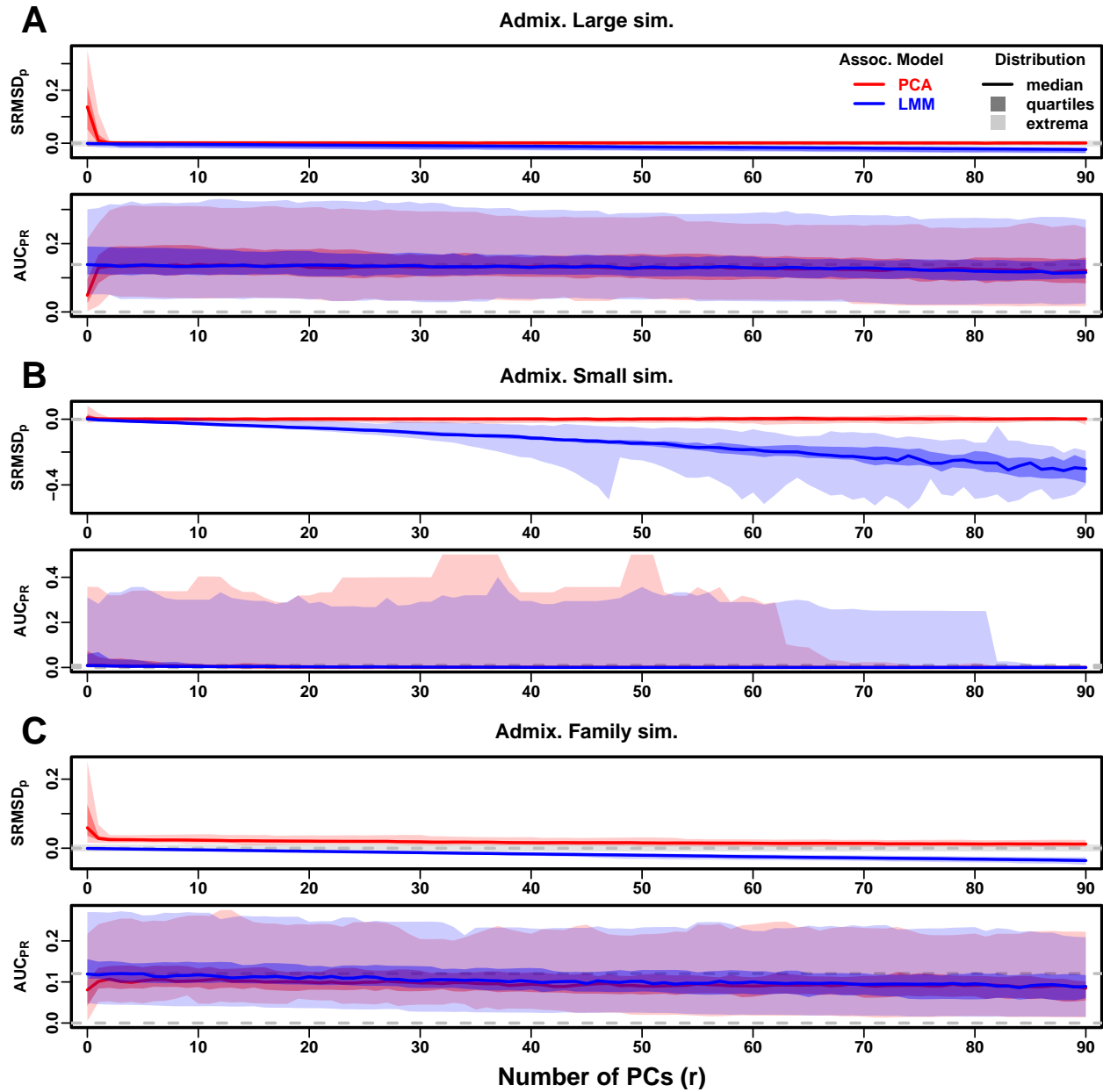


Figure S6: Evaluations in admixture simulations with FES traits, low heritability. Traits simulated using $h^2 = 0.3$, otherwise the same as Fig. 3.

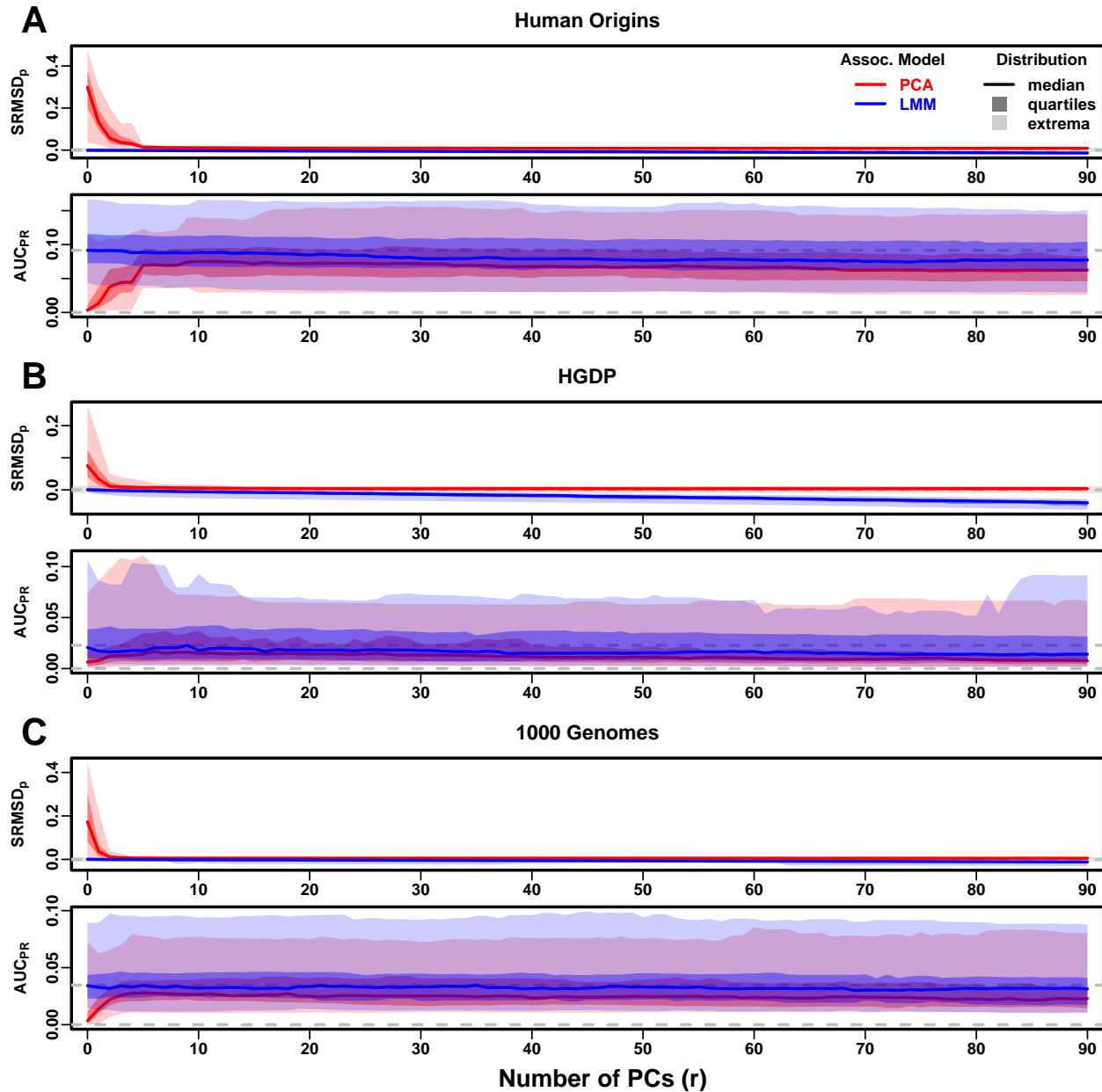


Figure S7: Evaluations in real human genotype datasets with FES traits, low heritability. Traits simulated using $h^2 = 0.3$, otherwise the same as Fig. 4.

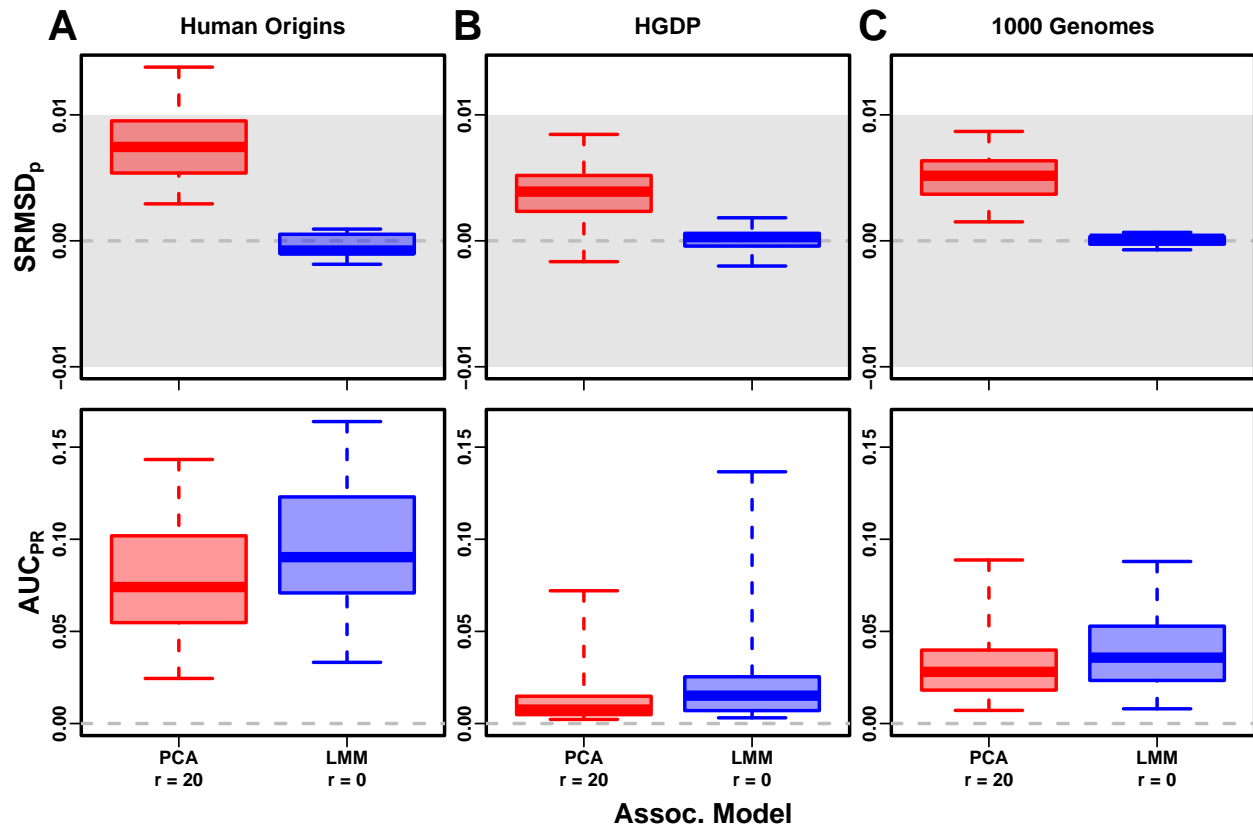


Figure S8: Evaluation in real datasets excluding 4th degree relatives, FES traits, low heritability. Traits simulated using $h^2 = 0.3$, otherwise the same as Fig. 7.

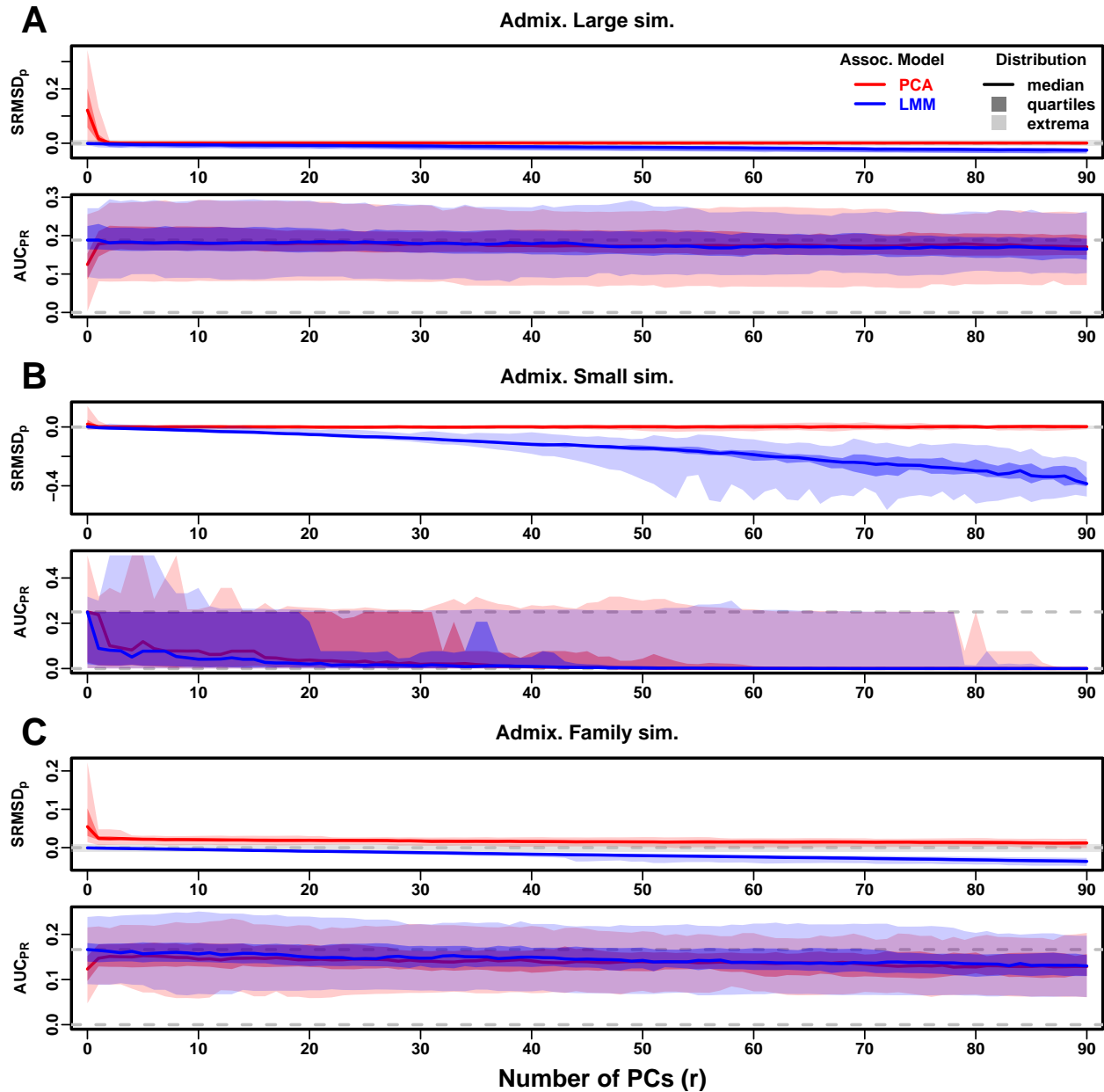


Figure S9: Evaluations in admixture simulations with RC traits, low heritability. Traits simulated using $h^2 = 0.3$, otherwise the same as Fig. S2.

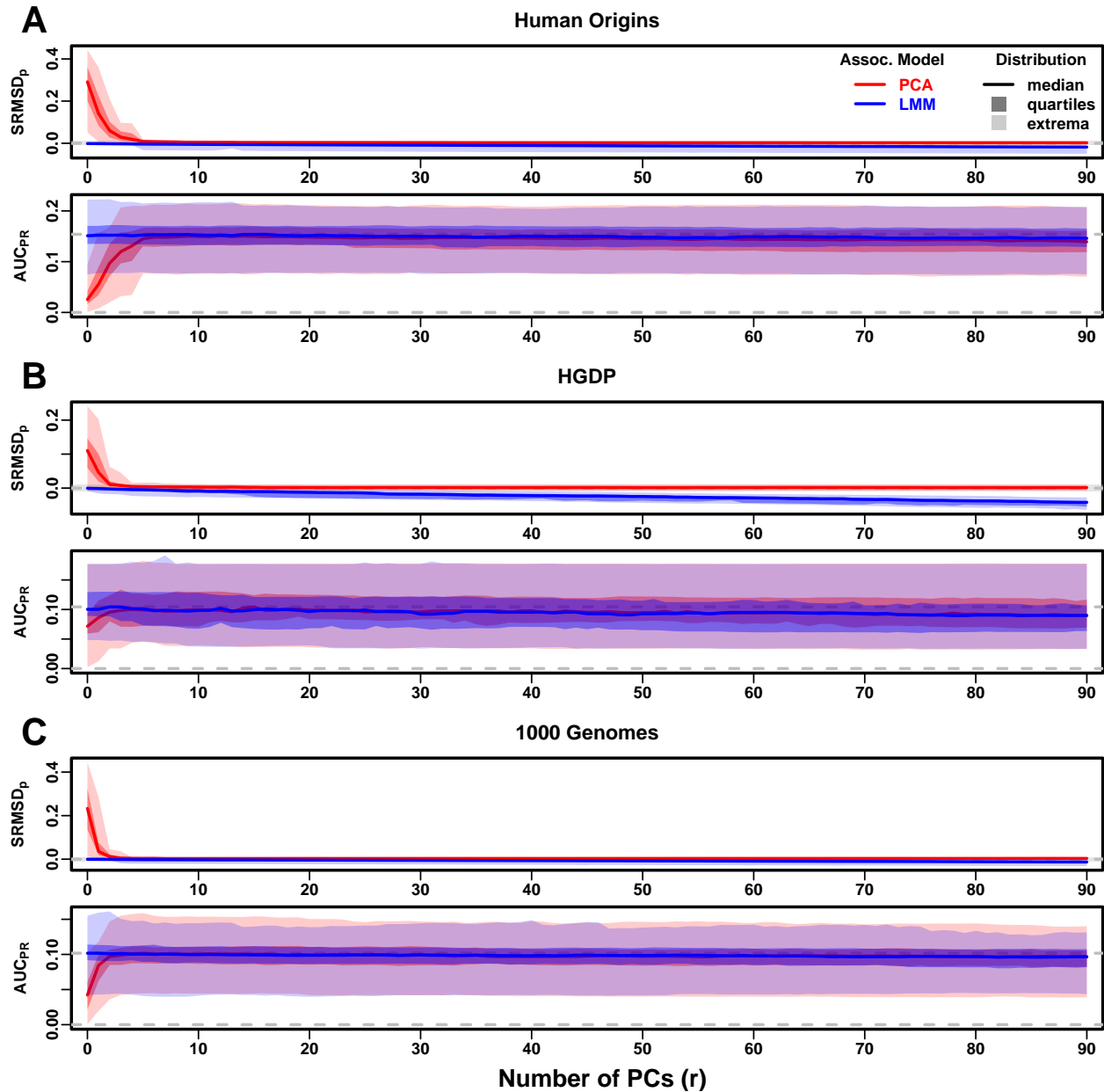


Figure S10: Evaluations in real human genotype datasets with RC traits, low heritability. Traits simulated using $h^2 = 0.3$, otherwise the same as Fig. S3.

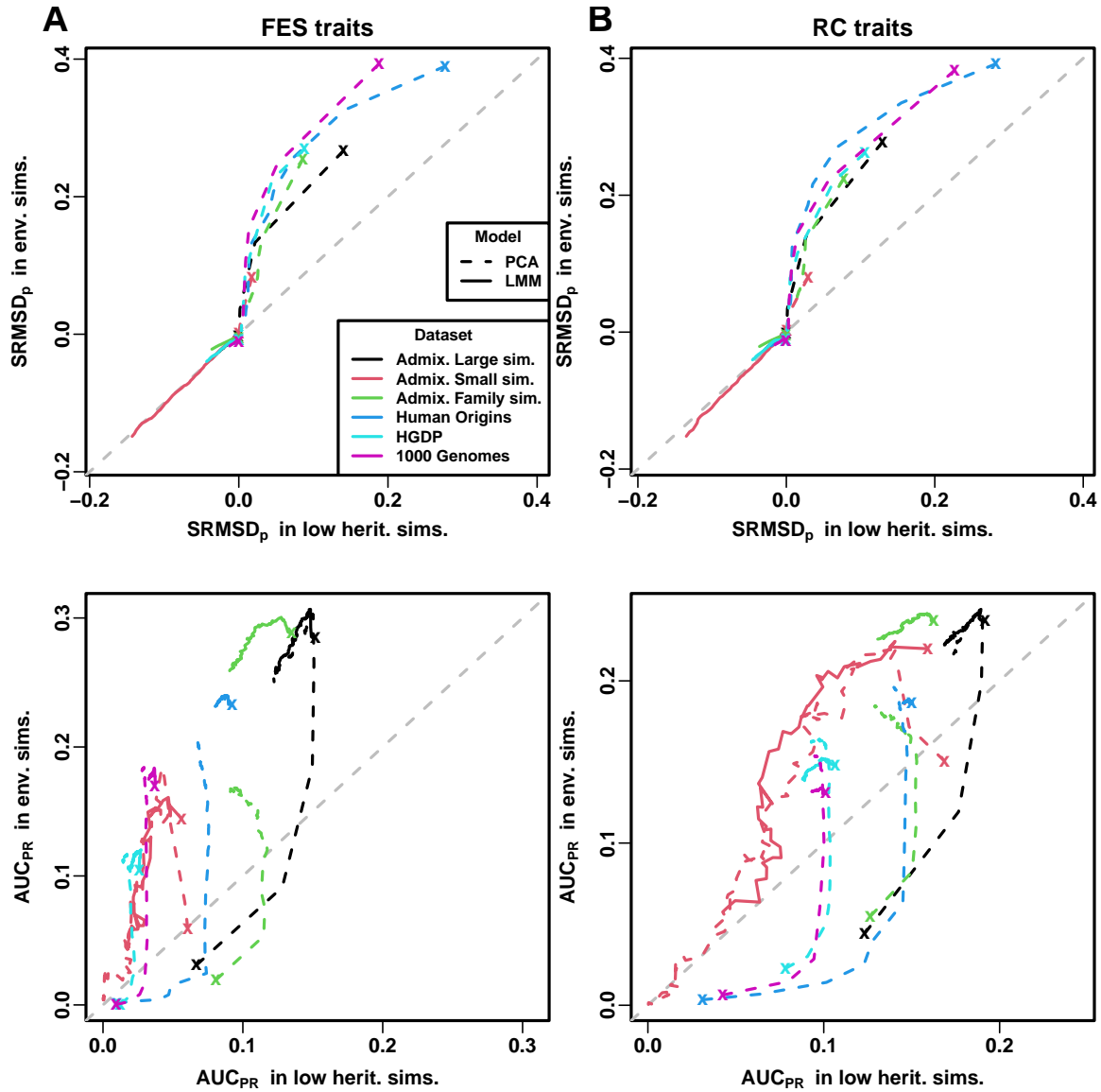


Figure S11: Comparison of performance in low heritability vs environment simulations. Each curve traces as the number of PCs r is increased from $r = 0$ (marked with an “ \times ”) until $r = 90$ (unmarked end), on one axis is the mean value over replicates of either SRMSD_p or AUC_{PR} , for low heritability simulations on the x-axis and environment simulations on the y-axis. Each curve corresponds to one dataset (color) and association model (solid or dashed line type). Columns: **A.** FES and **B.** RC traits show similar results. First row shows that for PCA curves SRMSD_p is higher (worse) in environment simulations for low r , but becomes equal in both simulations once r is sufficiently large; for LMM curves performance is equal in both simulations for all r , all datasets. Second row shows that for PCA curves AUC_{PR} is higher (better) in low heritability simulations for low r , but becomes higher in environment simulations once r is sufficiently large; for LMM curves performance is better in environment simulations for all r , all datasets.

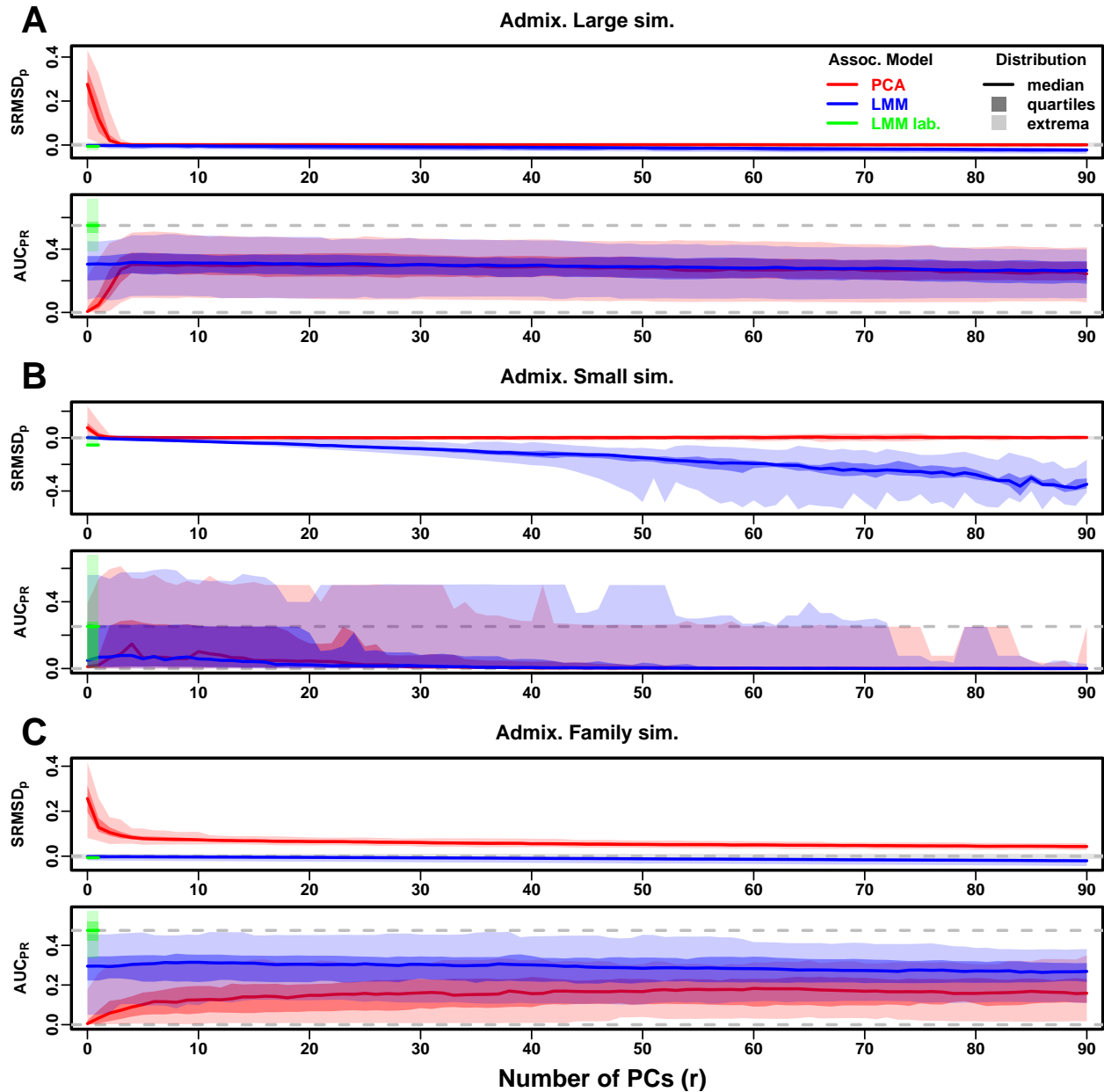


Figure S12: Evaluations in admixture simulations with FES traits, environment. Traits simulated with environment effects, otherwise the same as Fig. S6.

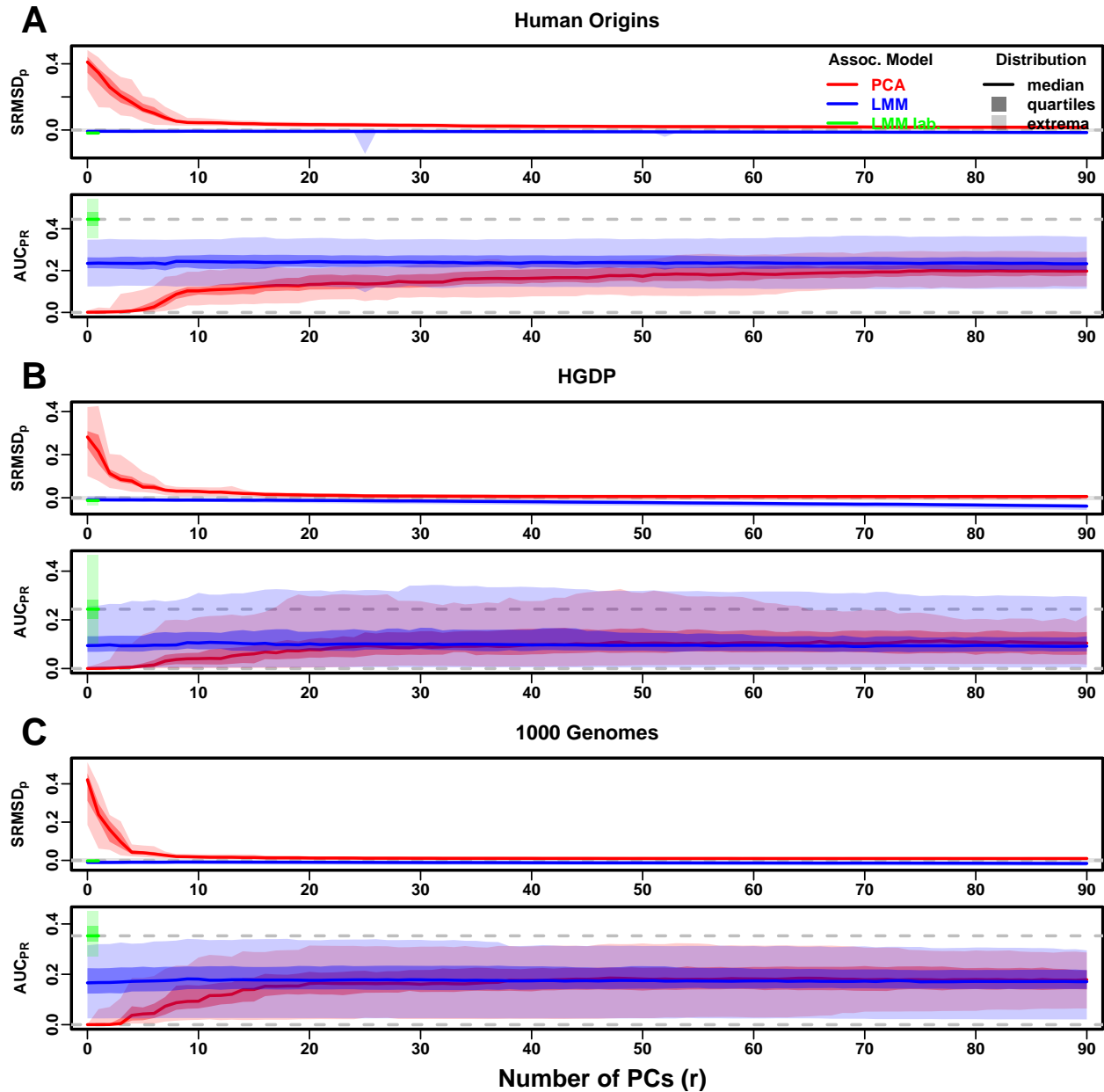


Figure S13: Evaluations in real human genotype datasets with FES traits, environment. Traits simulated with environment effects, otherwise the same as Fig. S7.

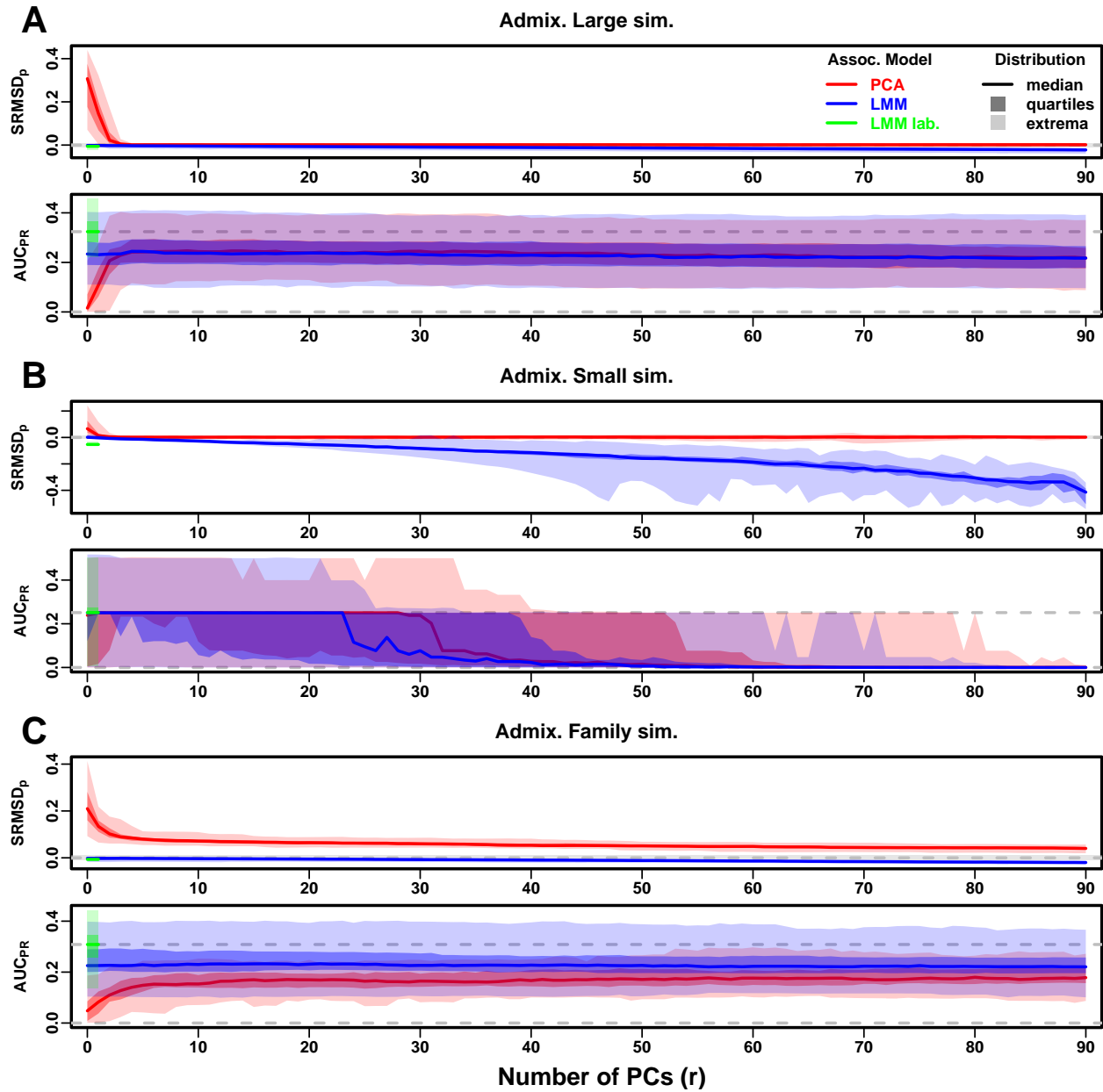


Figure S14: Evaluations in admixture simulations with RC traits, environment. Traits simulated with environment effects, otherwise the same as Fig. S9.

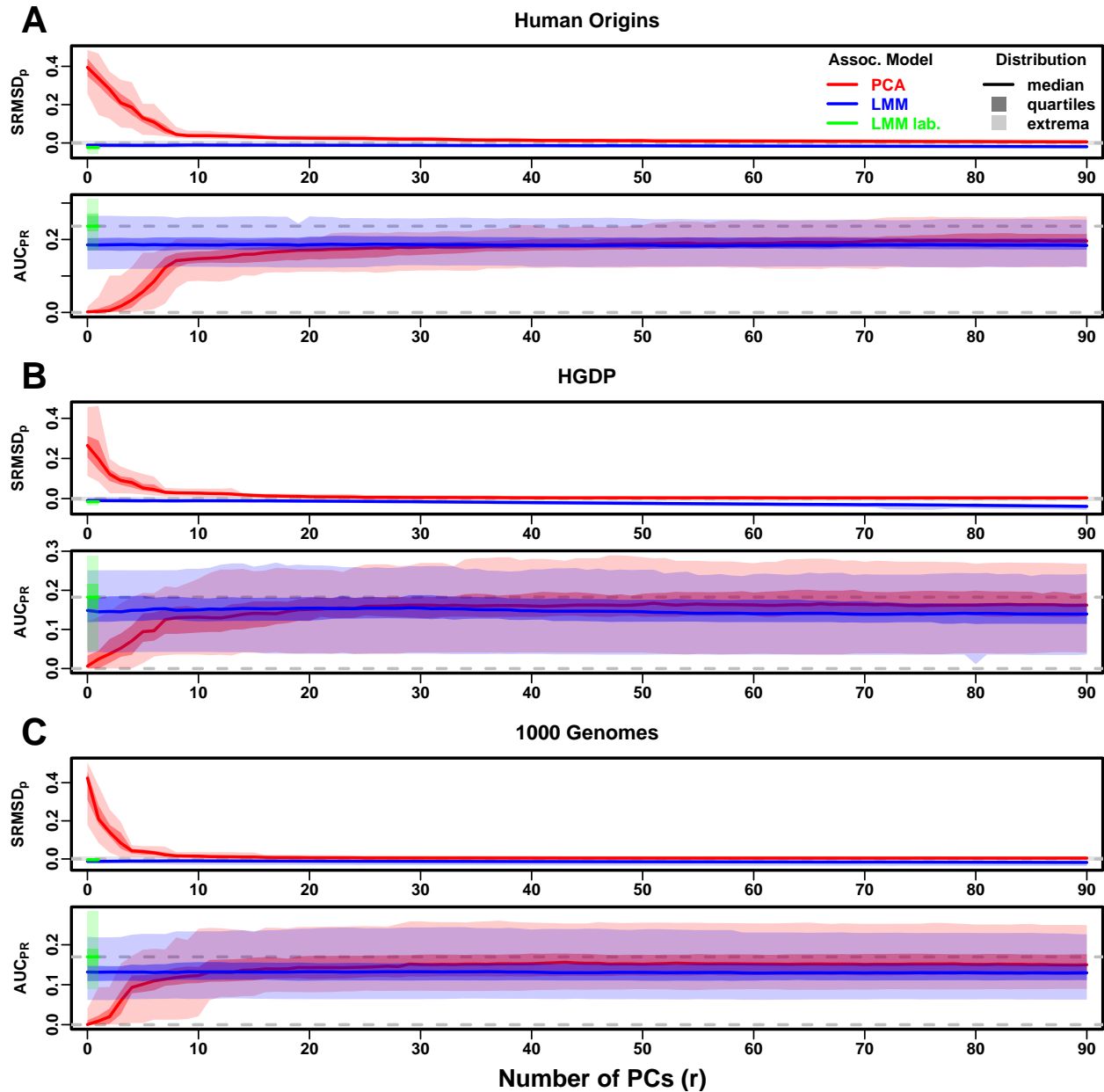


Figure S15: Evaluations in real human genotype datasets with RC traits, environment. Traits simulated with environment effects, otherwise the same as Fig. S10.

Supplemental tables

Table S1: Dataset sizes after 4th degree relative filter.

Dataset	Loci (m)	Ind. (n)	Ind. removed (%)
Human Origins	189,722	2636	9.8
HGDP	758,009	847	8.8
1000 Genomes	1,097,415	2390	4.6

Table S2: Overview of PCA and LMM evaluations for low heritability simulations

Dataset	Metric	Trait ^a	LMM $r = 0$ vs best r			Best r^c	PCA vs LMM $r = 0$		
			Cal. ^b	Best r^c	P-value ^d		Cal. ^b	P-value ^d	Best model ^e
Admix. Large sim.	$ \text{SRMSD}_p $	FES	True	0	1	62	True	0.00012*	LMM
Admix. Small sim.	$ \text{SRMSD}_p $	FES	True	0	1	3	True	0.27	Tie
Admix. Family sim.	$ \text{SRMSD}_p $	FES	True	0	1	90	False	3.9e-10*	LMM
Human Origins	$ \text{SRMSD}_p $	FES	True	0	1	81	True	3.9e-10*	LMM
HGDP	$ \text{SRMSD}_p $	FES	True	0	1	37	True	6.2e-09*	LMM
1000 Genomes	$ \text{SRMSD}_p $	FES	True	0	1	84	True	3.9e-10*	LMM
Admix. Large sim.	$ \text{SRMSD}_p $	RC	True	0	1	35	True	0.00094	Tie
Admix. Small sim.	$ \text{SRMSD}_p $	RC	True	0	1	3	True	0.087	Tie
Admix. Family sim.	$ \text{SRMSD}_p $	RC	True	0	1	90	False	4.1e-10*	LMM
Human Origins	$ \text{SRMSD}_p $	RC	True	0	1	75	True	0.00016*	LMM
HGDP	$ \text{SRMSD}_p $	RC	True	0	1	23	True	1.7e-05*	LMM
1000 Genomes	$ \text{SRMSD}_p $	RC	True	0	1	41	True	6.7e-10*	LMM
Admix. Large sim.	AUC _{PR}	FES	0	1		3		0.11	Tie
Admix. Small sim.	AUC _{PR}	FES	0	1		0		0.58	Tie
Admix. Family sim.	AUC _{PR}	FES	0	1		7		2.2e-06*	LMM
Human Origins	AUC _{PR}	FES	0	1		16		8e-10*	LMM
HGDP	AUC _{PR}	FES		11	0.68	6		0.0043	Tie
1000 Genomes	AUC _{PR}	FES		6	0.34	4		2.3e-07*	LMM
Admix. Large sim.	AUC _{PR}	RC	0	1		3		0.14	Tie
Admix. Small sim.	AUC _{PR}	RC	0	1		0		0.1	Tie
Admix. Family sim.	AUC _{PR}	RC	0	1		5		1.9e-06*	LMM
Human Origins	AUC _{PR}	RC	4	0.16		12		0.003	Tie
HGDP	AUC _{PR}	RC	2	0.14		5		0.14	Tie
1000 Genomes	AUC _{PR}	RC	0	1		4		0.078	Tie

^aFES: Fixed Effect Sizes, RC: Random Coefficients.

^bCalibrated: whether mean $|\text{SRMSD}_p| < 0.01$.

^cValue of r (number of PCs) with minimum mean $|\text{SRMSD}_p|$ or maximum mean AUC_{PR}.

^dWilcoxon paired 1-tailed test of distributions ($|\text{SRMSD}_p|$ or AUC_{PR}) between models in header. Asterisk marks significant value using Bonferroni threshold ($p < \alpha/n_{\text{tests}}$ with $\alpha = 0.01$ and $n_{\text{tests}} = 48$ is the number of tests in this table).

^eTie if no significant difference using Bonferroni threshold.

Table S3: Overview of PCA and LMM evaluations for environment simulations

Dataset	Metric	Trait ^a	LMM $r = 0$ vs best r			PCA vs LMM $r = 0$			LMM lab. vs PCA/LMM		
			Cal. ^b	r^c	P-value ^d	r^c	Cal. ^b	P-value ^d	Best ^e	Cal. ^b	P-value ^d
Admix. Large sim.	$ \text{SRMSD}_p $	FES	True	0	1	83	True	0.38	Tie	True	1.8e-14*
Admix. Small sim.	$ \text{SRMSD}_p $	FES	True	0	1	90	True	0.001	Tie	False	1.4e-14*
Admix. Family sim.	$ \text{SRMSD}_p $	FES	True	4	0.18	90	False	3.9e-10*	LMM	True	0.066
Human Origins	$ \text{SRMSD}_p $	FES	True	9	3.9e-05*	90	False	1.4e-08*	LMM	False	3.9e-10*
HGDP	$ \text{SRMSD}_p $	FES	True	0	1	90	True	0.0037	Tie	False	2.1e-09*
1000 Genomes	$ \text{SRMSD}_p $	FES	False	8	8.8e-08*	85	True	0.053	Tie	True	3.9e-10*
Admix. Large sim.	$ \text{SRMSD}_p $	RC	True	0	1	60	True	0.033	Tie	True	6.3e-10*
Admix. Small sim.	$ \text{SRMSD}_p $	RC	True	0	1	9	True	0.85	Tie	False	1.4e-14*
Admix. Family sim.	$ \text{SRMSD}_p $	RC	True	5	0.14	90	False	3.9e-10*	LMM	True	0.011
Human Origins	$ \text{SRMSD}_p $	RC	False	9	1.1e-08*	90	True	2.3e-07*	PCA	False	3.9e-10*
HGDP	$ \text{SRMSD}_p $	RC	True	0	1	89	True	6.5e-09*	PCA	False	3.9e-10*
1000 Genomes	$ \text{SRMSD}_p $	RC	False	8	1.6e-08*	88	True	4.9e-09*	PCA	True	0.09
Admix. Large sim.	AUC _{PR}	FES		4	2.4e-06*	6		0.0021	Tie		1.8e-15*
Admix. Small sim.	AUC _{PR}	FES		3	0.055	4		0.033	Tie		0.28
Admix. Family sim.	AUC _{PR}	FES		12	7e-04	63		3.9e-10*	LMM		3.9e-10*
Human Origins	AUC _{PR}	FES		20	3.7e-06*	90		1.4e-05*	LMM		3.9e-10*
HGDP	AUC _{PR}	FES		12	4.3e-06*	45		0.0044	Tie		3.9e-10*
1000 Genomes	AUC _{PR}	FES		9	1.9e-08*	55		0.028	Tie		3.9e-10*
Admix. Large sim.	AUC _{PR}	RC		4	0.00085	5		0.0018	Tie		5e-10*
Admix. Small sim.	AUC _{PR}	RC		2	0.13	5		0.093	Tie		0.0028
Admix. Family sim.	AUC _{PR}	RC		9	0.01	86		1.7e-09*	LMM		3.9e-10*
Human Origins	AUC _{PR}	RC		22	0.0039	90		1e-06*	PCA		3.9e-10*
HGDP	AUC _{PR}	RC		19	0.0057	64		2.8e-05*	PCA		3e-07*
1000 Genomes	AUC _{PR}	RC		9	8.7e-05*	87		1.2e-09*	PCA		4.4e-10*

^aFES: Fixed Effect Sizes, RC: Random Coefficients.

^bCalibrated: whether mean $|\text{SRMSD}_p| < 0.01$.

^cValue of r (number of PCs) with minimum mean $|\text{SRMSD}_p|$ or maximum mean AUC_{PR}.

^dWilcoxon paired 1-tailed test of distributions ($|\text{SRMSD}_p|$ or AUC_{PR}) between models in header. Asterisk marks significant value using Bonferroni threshold ($p < \alpha/n_{\text{tests}}$ with $\alpha = 0.01$ and $n_{\text{tests}} = 72$ is the number of tests in this table).

^eTie if no significant difference using Bonferroni threshold; in last column, pairwise ties are specified and “Tie” is three-way tie.